NOVEL DETECTION AND DETERMINATION OF ANALYTES IN THE MOLAR SOLUTION DOMAIN

Stuart Licht

Department of Chemistry
Technion Israel Institute of Technology
Haifa, 32000, Israel

CONTENTS:

I. INTRODUCTION

Solution phase methodologies have focused on analysis of dilute solutions for both pragmatic and fundamental reasons. The magnitude of conventional spectroscopic extinction coefficients, dictates that concentrated solutions tend to be opaque; precluding conventional absorption spectroscopy of solutions containing molar concentrations. Electrochemical methods are limited in concentrated solutions due to uncertainties including ill defined liquid junction potentials, electrode instability, and solution activity. From a fundamental perspective, Debye-Hückel theory breaks down, and activity coefficients can deviate substantially from unity in concentrated solutions.

Yet, conventional spectroscopic, electrochemical and chromatographic methodologies are often not suitable to probe chemistry in the concentrated solution phase. In industrial, environmental and many synthetic and research processes, highly concentrated solutions are prevalent. In order to analyze concentrated solutions, most conventional

methodologies require an initial solution dilution step. However, this dilution step precludes measurement of interesting complexation, association, or solvent driven equilibria which can occur in the concentrated phase. There are few, direct or *in-situ* analytical methodologies for analysis of these highly concentrated electrolytes. Instead, analysis of these solutions is often accomplished with extraction and dilution steps. From a practical perspective, dilution steps can lengthen analysis time, add contaminants, and provide only incomplete information regarding chemical interactions in a concentrated solution.

This paper presents five methodologies, three electrochemical and two chemical in nature, which are suitable for analysis of concentrated solutions. The electrochemical methodologies are variations of electroanalytical or ionic methods and are entitled: Concentrated Solution Potentiometric Analysis, Evanescent (Solvent) Activity Analysis, and a third, Differential Conductometric Analysis Section II probes fundamental and practical issues related to Potentiometric Analysis (ion selective electrode methodologies) including solutions over 10 molal in concentration, and compares theoretical derivation and experimental determinations of aqueous pH values of over 17. Section III presents a dynamic technique to determine activities of concentrated electrolytes. This Evanescent Analysis correlates induced evaporative mass loss of solution with solvent and solution activity. Ionic conductivity which is enhanced, rather than obscured, with increasing electrolyte provides a precise probe of concentrated electrolytes. This is the framework for Differential Conductometric Analysis in Section IV, in which speciation is determined by comparing the conductivity of isolated reactants with that of an equilibrated homogeneous mixture.

In addition to the three electrochemical methodologies, two chemical methodologies are investigated, techniques which can be appropriate for the analysis of concentrated media (solutions of 0.1 to over 10 molar in analyte). The variation of several physical chemical phenomenon are accentuated in increasingly concentrated solution and, in principal, may be the basis for analytical probes and methodologies in these solutions. One methodology, discussed in Section V, Differential Densometric Analysis, takes advantage of such a physical chemical property (density) [1,2]. In concentrated solutions, the solute comprises a significant mole fraction of the electrolyte, and density variations can be used to gauge equilibria. A final methodology, Sub-micron Path UV/Vis/IR Spectroscopy, discussed in Section VI, uses a specialized spectroscopic cell in which the cell path length can be shorter than the wavelength of incident light through the cell [2,3].

II. POTENTIOMETRIC ANALYSIS

A. Conventional pH Measurement

The conventional domain of aqueous pH analysis generates and evaluates pH values in the range of 0 to 14. pH is traditionally defined from the hydrogen ion activity, a_{H^+}:

$$pH = -\log(a_{H^+}) \quad (1)$$

In solutions dominated by hydroxide ions it is convenient to rewrite equation (1) with inclusion of the equation describing the water dissociation constant, K_w:

$$K_w = a_{H^+} \ \gamma_{OH^-} \mathbf{m}_{OH^-} / a_w; \qquad K_w(25^oC) = 14.00 \quad (2)$$

where at the hydroxide molal concentration, $\mathbf{m}_{OH^-}$, the hydroxide activity coefficient is γ_{OH^-} and the water activity coefficient is a_w, (a_w and $\gamma_{OH^-} = 1$ in 55.508 **m** (pure) water). Upon substitution of equation (2), equation (1) yields:

$$pH(25^oC) = 14.00 + \log(\gamma_{OH^-} \mathbf{m}_{OH^-} / a_w) \quad (3)$$

Individual redox half cells can not be fully isolated, and therefore individual ion activity coefficients cannot be precisely measured. Hence, measurement of pH in accord with equations (1) or (3) is problematic. However, the potential of a full cell may be measured, for example using a potentiometric cell consisting of a sensing electrode and a reference electrode immersed in electrolyte:

$$\text{pH electrode} \mid \text{sample solution} \mid E_{\text{reference electrode}} \quad (4)$$

In addition to the desired response to pH, the potential of the cell expressed by equation (4) can have uncertainty from the possible response to interferring ions, E_c, at the pH electrode and to liquid junction potentials, E_j at the reference electrode interface:

$$E_{H^+} = E^o_{H^+} + S \log (a_{H^+}) - E_j - E_c \quad (5)$$

leading to the further necessity of an operational definition of pH according to the convention of Bates [4]:

$$pH_{measured} = pH_{standard} + (E_{H^+} - E_{ref})/ S \quad (6)$$

where (E_{H+} - E_{ref}) is the differential voltage measured between the pH and the reference electrode. The slope, S, is the measured differential voltage response with pH of the electrode (typically, S(volts) = 17.64/T(K) per pH unit or approximately 0.059 V at 25°C). $pH_{standard}$ is the defined pH of a standardizing solution used to calibrate the potential response of the cell; several pH standardizing solutions are available [4].

pH measurement is one of the most widely used analytical technques, and the conventional cell configuration of equation (4) is found in chemistry, biology and environmental laboratories throughout the world. This generally consists of a single probe containing both a glass pH electrode and a reference electrode in close proximity, with their potential difference measured by a high input impedance voltammeter necessary due to the high resistivity of the glass ion selective electrode.

B. Colorimetric Estimates of pH in Concentrated Acids and Bases

In highly concentrated (over 1 normal) acidic or alkaline solutions, pH values are expected to range beyond the conventional bounds of $0 < pH < 14$. Colorimetric techniques have been employed to estimate pH in concentrated acid and concentrated alkaline solutions [5,6], and generally employ absorption spectroscopy to evaluate an equilibrium which is influenced by hydrogen ion activity. By studying a relatively dilute indicator species, these techniques bypass the problems of high absorbance expected if the concentrated analyte (in this case H^+ or OH^-) was directly observed. However, these techniques are limited by problems arising from solution oxidation/reduction of the dilute indicator, overlapping absorbance by other speices or colloidal suspensions [7]. In addition, these techniques are indirect. Rather than measure pH, they measure chromophores whose concentration are affected by pH. For identical solutions, the different colorimetric techniques can been shown to estimate hydrogen ion activities which vary by several orders of magnitude in both acidic and basic media [8] depending on which indicator is utilized, and generally are related to the correct pH only by an indeterminate constant [9].

C. Calculation of pH in Concentrated Acids and Bases

The theoretical foundation for understanding of pH becomes increasingly problematic in concentrated solutions. The fundamental definition of pH, equation (1), is based on the hydrogen ion activity.

However, single ion activities are experimentally inaccessible, and are expected to deviate substantially from unity in concentrated electrolytes.

Whereas, single ion activities are experimentally inaccessible, this is not the case for mean solution activities which have been well characterized for acidic and alkaline solutions. These experimentally reproducible, fundamental values for solution activity provide a basis for a modified definition of pH, in which equations (1) and (3) are modified to incorporate these measurable parameters. For example with alkali hydroxide salt solutions, equation (3), may be modified to calculate pH from known mean solution activities, $a_{+} = a_{KOH} = \gamma_{\pm MOH}\, \mathbf{m}_{MOH}$, $\gamma_{\pm MOH}$ = activity coefficient in solution of concentration $\mathbf{m}_{MOH}$, and at 25°C [8]:

$$pH_{calculated} = 14.00 + \log(\gamma_{\pm MOH} \mathbf{m}_{MOH} / a_w) \qquad (7)$$

pH values substantially beyond 14 can exist in aqueous solutions. Debye-Hückel theory indicates that activity coefficients approach unity at low concentrations. However, very concentrated aqueous alkali hydroxide solutions are known to have mean solution activity coefficients which can reach more than an order of magnitude higher ; indeed, nearly saturated, highly concentrated sodium or potassium hydroxide solutions have mean solution activities greater than 30 [8]. In these solutions the majority of the water is bound within the sphere of ionic hydration and the water activity drops to less than 0.2. Thus the value of $\gamma_{\pm MOH} / a_w$ can be larger than 100, and from equation (7) for solutions over 10 molal, pH values larger than 17 are expected.

Table 1 presents calculated pH values for a range of potassium hydroxide electrolytes. For example, at 25°C in respective 3.0 **m** and 17.5 m KOH solutions, a_{KOH} increases from 3.18 to 602, and a_w decreases from 0.872 to 0.143 [10]. In accordance with equation (7) this leads to predicted pH values of 14.66 and 17.62 respectively in 3.0 m and 17.5 **m** KOH solutions. Equation (7) provides a consistent fundamental basis to predict pH of highly concentrated alkaline solutions. Unusually high pH values are expected, and as demonstrated in the next section, these can be experimentally measured and verified.

D. Potentiometric Measurement of pH in Concentrated Alkaline Solutions

Several obstacles must be considered in potentiometric measurement of concentrated electrolytes. These are (i) competitive ion interference, (ii) liquid junction potential errors, and (iii) chemical attack of the sensor electrode. Effects of competitive ion interference will occur as cation errors in alkali pH measurement. High cation concentrations, for example K^+ in KOH or Ba^{2+} in $BaOH_2$, are necessary

TABLE 1. The calculated pH of aqueous KOH solutions at 25°C, determined from equation (7) using data from references 8 and 10. The mean solution activities, $a_{\pm} = a_{KOH}$ is determined as the product of $\gamma_{\pm MOH}$ and m_{MOH}.

m_{KOH}	$\gamma_{\pm KOH}$	a_w	$\log(a_{KOH}^2/a_w)$	$pH_{calculated}$
0.000100	0.99	1.00	-8.01	10.00
0.00100	0.97	1.00	-6.03	10.99
0.0100	0.91	1.00	-4.04	11.96
0.100	0.99	1.00	-2.20	12.90
0.300	0.74	0.99	-1.30	13.35
1.00	0.75	0.96	-0.23	13.89
3.00	1.06	0.872	1.06	14.66
4.50	1.51	0.790	1.77	14.93
6.00	2.22	0.700	2.40	15.28
7.50	3.29	0.604	3.00	15.61
9.00	4.86	0.508	3.58	15.94
10.5	7.10	0.419	4.12	16.25
12.0	10.2	0.342	4.64	16.55
13.5	14.5	0.278	5.14	16.85
15.0	20.2	0.221	5.62	17.14
16.0	25.0	0.187	5.93	17.33
17.0	30.9	0.157	6.24	17.52
17.5	34.4	0.143	6.40	17.62

to introduce high hydroxide concentration. In increasingly concentrated alkali solutions as the solvated proton concentration diminishes, these other cation concentrations increase, and can increasingly influence the potential of the pH electrode.

The sensing element of commercially available pH electrodes is comprised of glasses of various compositions. The magnitude of the cation error for these pH electrodes varies with glass composition and cation type in solution. However, for example, in a sodium hydroxide solution, it typically generates on the order of a 1 to 2 pH unit underestimate of the pH in a 1 m NaOH solution. Various commercial ion selective electrode manufacturers have specific glass sensor compositions comprised to minimize the magnitude of cation error in alkaline solutions [4,7]. Cation errors can be substantially less in alkaline potassium solutions, compared to sodium electrolytes, providing an effective medium to determine and monitor concentrated pH [8]. Other commercial glass compositions have been chosen to minimize the response to hydrogen ion and maximize the

response to alkali or alkali hydroxide cations to create cation sensing ion selective electrodes. In concentrated alkaline solutions, these electrodes effectively respond exclusively to the cation salt activity (competitive ion interference due to the extremely low hydrogen ion activity is then not significant).

When a cation selective potentiometric electrode is available, the interference on a pH electrode due to this cation can be quantified. For example, the potassium ion error at a pH electrode may be determined by potentiometric measurement of the cell:

$$E_{\text{potassium electrode}} \mid \text{sample solution} \mid \text{pH electrode} \qquad (8)$$

Whereas, the potentials of either pH or potassium electrode cells contain uncertainties in individual ion activities and liquid junction potentials, equations (5) and (9), this is not the case for the potential of the combined cell (8) which is denoted $E_{K+} - E_{H+}$.

$$E_{K+} = E^{\circ}_{K+} + S \log (a_{K+}) - E_j \qquad (9)$$

As derived from equations (2), (5) and (9), the potential of cell (7) is expected to vary with $\log (a_{KOH}^2 / a_w)$ [8]. The nonlinear variation of $E_{K+} - E_{H+}$ with $\log (a_{KOH}^2 / a_w)$ provides a measure of the cation error on the pH electrode, E_c, for this cell:

$$E_{K+} - E_{H+} = \text{a constant} + S \log (a_{KOH}^2 / a_w) + E_c \qquad (10)$$

Figure 1 presents the potential difference measured between pH and K^+ selective glass electrodes in both dilute and highly concentrated potassium hydroxide solutions. As seen in the figure, using this commercial low cation error pH electrode, voltage deviations from linearity are small for concentrations up to 6 m KOH ($\log (a_{KOH}^2 / a_w) = 2.4$), but then rises to 0.05 V, equivalent to an 0.8 pH unit cation error in a 17.5 m KOH ($\log (a_{KOH}^2 / a_w) = 6.4$), electrolyte.

The pH measuring cell represented by equation (4) contains a reference electrode which can present a second uncertainty to pH measurement of concentrated electrolytes. A conventional reference electrode, such as either the saturated calomel or the silver chloride reference electrodes commonly employed, contains an internal solution separated from the analyte solution by either a ceramic frit, gel, membrane, small orifice or other flow impeding mechanism. The ion activity differential between the sample and internal reference solutions gives rise to a liquid junction potential, E_j, which is expected to vary as different sample solutions are probed by the pH cell of equation (4). The calculation of E_j is highly problematic as evidenced by an order of

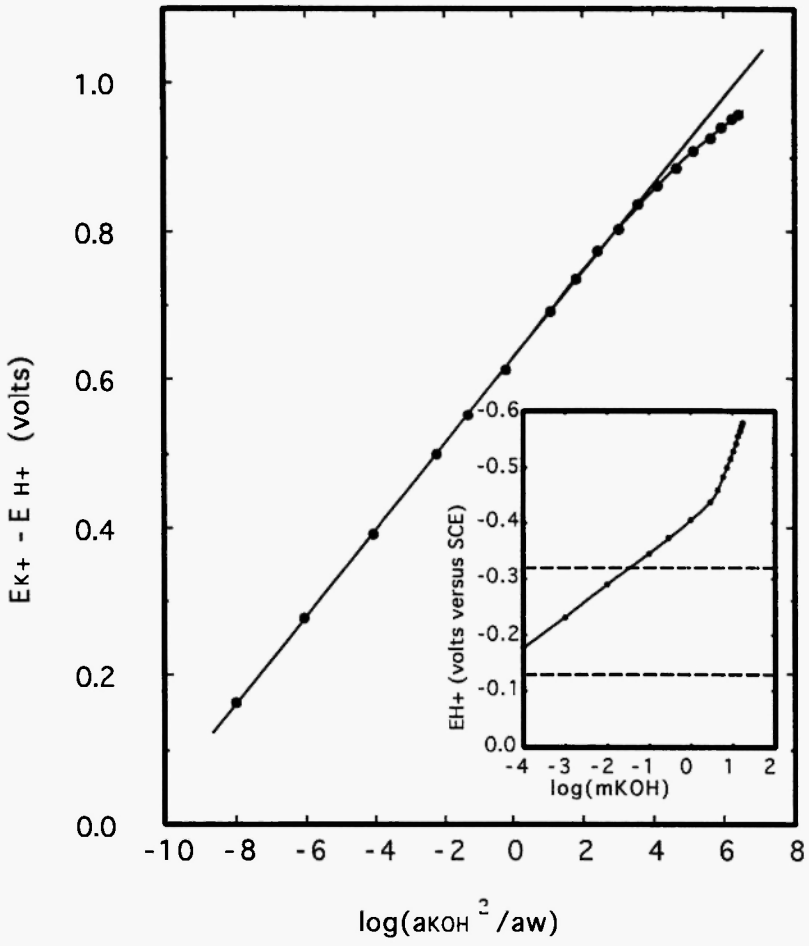

FIGURE 1 The voltage of an liquid junction potential free potassium hydroxide cell as a function of log (a_{KOH}^2 /a_w) at 25°C. The cell is comprised of a Radiometer G202BH pH electrode measured versus a Beckman 39317 cation selective electrode immersed in solutions varying from 10^{-4} to 17.5 **m** KOH. Cell potential is measured with a conventional high input impedance voltammeter. Figure inset: The voltage response of a low cation error pH cell as a function of potassium hydroxide concentration at 25°C. The cell is comprised of a Radiometer G202BH pH electrode measured versus a Radiometer K401 saturated calomel electrode immersed in solutions varying from 10^{-4} to 17.5 **m** KOH. Cell potential is measured with a conventional high input impedance voltammeter. The upper and lower dashed lines are the potentials measured respectively in saturated calcium hydroxide and 0.1 **m** borax solutions. From reference 8.

magnitude difference in predicted liquid junction potentials even between simple monovalent salt solutions [4,11,12,13]. In one estimate, Picknett observes a correspondence of E_j to solution specific conductivity [12]. His model does not require the additional assumption of the Henderson model [4] which had assumed a specific ionic distribution in the liquid junction region. Picknett estimates E_j variation between KOH and KCl solutions to vary linearly with concentration and to generate a small potential of approximately 1 mV per decade differential in concentration [12].

The inset of Figure 1 presents the potential response, E_{H+}, of a low alkali error pH cell as a function of concentration in KOH solutions at 25°C. In the figure, the upper dashed line represents measured E_{H+} in a saturated calcium hydroxide solution with known pH of 12.454, further calibrated with a 0.0100 m borax solution (with a defined primary pH standard of 9.180). At high pH the measured cation interference be used to correct the measured pH, and the operational definition of pH may be modified to incorporate this cation error potential:

$$pH_{measured} = pH_{standard} + (E_{H+} - E_{ref})/ S + E_c / S \quad (11)$$

Using the measured values of E_{H+} presented in the inset of Figure 1, values of $pH_{measured}$, have been determined without cation correction from equation (6), and also determined with the cation correction values of E_c from Figure 1 and equation (10). Figure 2 presents the resultant comparison of $pH_{measured}$ to theoretical pH values calculated and summarized in Table 1 as $pH_{calculated}$. Closed circle points are for $pH_{measured}$ prior to cation correction; open circle points include the cation correction of E_c / S from equation (11). In this figure, it is seen that $pH_{measured}$ provides an highly linear estimate of the solution pH. With appropriate cation correction of E_c / S, the maximum deviation for $pH_{measured}$ is ~0.1 pH units. This small deviation is consistent with the low values of liquid junction potential error which would be predicted by the Picknett model [12].

Due to the relatively small ion interferences, potassium electrolytes provide an attractive media for the measurement of pH in highly alkaline solutions. However, it is also of interest to measure the magnitude of other cation interferences. The left side of Figure 3 presents measured sodium ion errors at 25°C for high pH values. Various concentrations of sodium chloride were added to 1.0, 4.5, 9.0 and 17.5 m potassium hydroxide solutions and the pH measured with a low cation error commercial pH electrode. In the figure, the dashed lines represent the pH of the sodium salt-free solutions. Analogous experiments were done lithium chloride to determine the magnitude of the pH depression which results from the presence of lithium ions. These results are shown in the right side of Figure 3. Lithium ion interference errors are larger

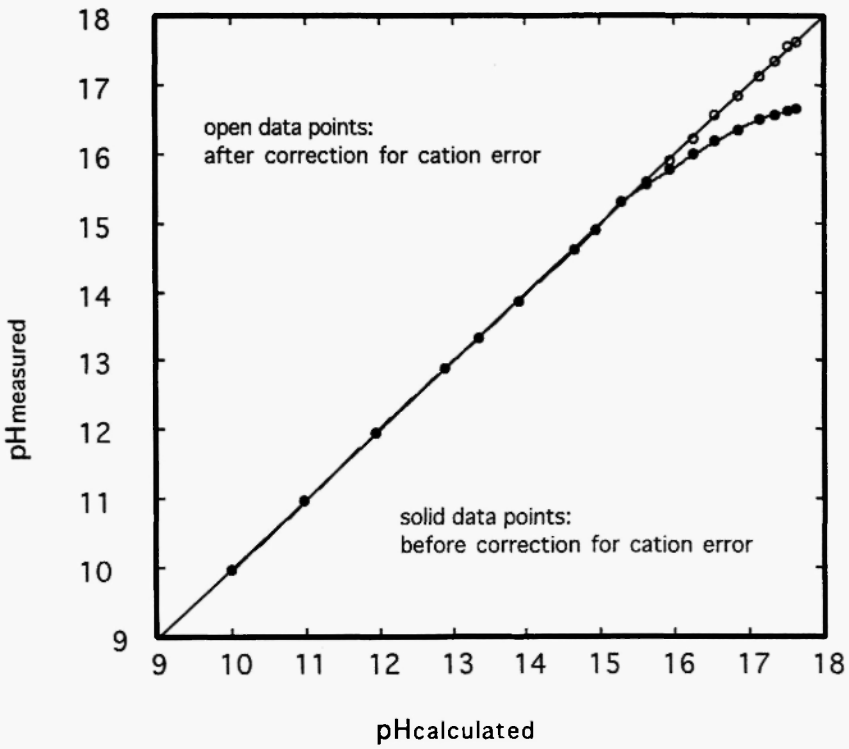

FIGURE 2 Potentiometric pH measurement in concentrated aqueous KOH solutions at 25°C. Predicted pH, $pH_{calculated}$, is compared to measured pH before (solid data points) and after (open data points) correction for cation error. From reference 8.

than sodium ion errors which in turn are substantially larger than potassium ion errors. It is evident from Figure 2, that these pH errors, due to the presence of relatively high known concentrations of lithium (up to 0.1 **m**) and sodium (up to 1 **m**) , may be compensated for even in highly alkaline solutions, if the primary cation is potassium and a low cation error pH electrode is used.

Despite the known alkali attack on glass, pH measurement can be shown to be stable on the order of hours in highly concentrated alkaline solutions. In glass, alkalis break the silicon oxygen bonds in the bridge network resulting in the dissolution of water-soluble silicates [14,15]. At higher temperature (80°C), significant dissolution of pH-sensitive glass has been observed to occur in one normal sodium, lithium potassium,

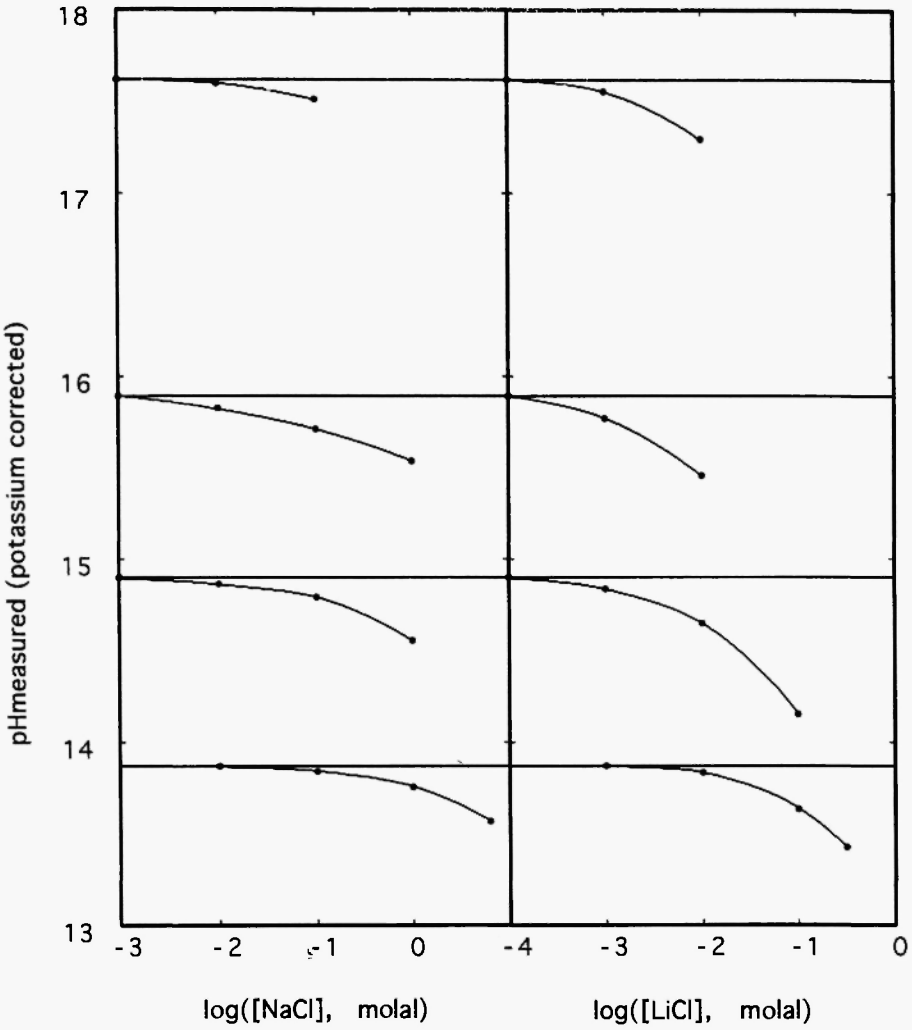

FIGURE 3 Left: Measured sodium errors for a Radiometer G202BH pH electrode in 1.0 (lowest curve), 4.5, 9.0, (lowest curve) 17.5 **m** KOH solutions as a function of added NaCl at 25°C. The pH cell is described in the legend of Figure 2. The dashed lines represents the sodium free solutions. Right: Measured lithium errors for a Radiometer G202BH pH electrode in 1.0 (lowest curve), 4.5, 9.0, (lowest curve) 17.5 **m** KOH solutions as a function of added LiCl at 25°C. The pH cell is described in the legend of Figure 2. The dashed lines represents the lithium free solutions. Modified from reference 8.

barium and ammonium hydroxide solutions. The greatest rate of dissolution was for the sodium solution and followed the order Na > Li > K > Ba > NH_4 [16]. No studies have been previously reported regarding the attack of pH sensitive glass in solutions of higher alkalinity or lower temperature. In Figure 4 is presented the measured pH in 17.5 m KOH at 25°C with a commercial pH electrode as a function of time. As seen in the figure, the pH for this electrode (a Radiometer G202BH electrode)

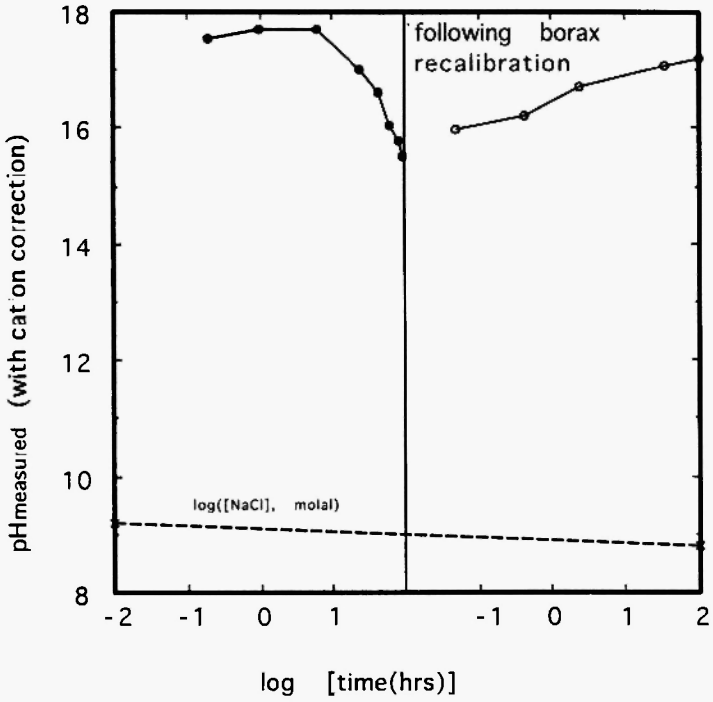

FIGURE 4 pH measurement in concentrated 17.5 **m** KOH solutions as a function of time at 25°C. The pH cell is described in the legend of Figure 2. The open circles represent individual measurements made during continual immersion of the pH electrode in the concentrated KOH solution. The reference electrode was only placed in the solution during pH measurement, and otherwise was in a saturated KCl solution. Closed circles represent individual subsequent measurements performed after soaking the pH electrode in distilled water for the indicated time. The dashed line represents the pH of an 0.01 m borax solution measured at the beginning and then at the conclusion of the experiment. Modified from reference 8.

remained relatively constant for the first 6 hours immersion in concentrated KOH followed by a decrease of 2.1 pH units by the hundredth hour. However, the pH returned to within ~0.1 pH units of the original value, as measured versus a 0.01 m borax reference after the electrode was rinsed then soaked for 100 hours in distilled water.

E. Theoretical and Experimental Tools for Concentrated Solution Potentiometric Analysis

The systematic use of mean solution activities, rather than colorimetric indicators or single ion activities, provides a consistent formalism for the prediction of solution interactions in concentrated electrolytes. Applying this formalism to pH, as shown for concentrated alkali solutions using equation (7), aqueous pH values substantially outside the conventional pH range of 0 to 14 are expected. For potassium hydroxide solutions these pH values range to over a pH of 17, as summarized in Table 1. The pH of these concentrated solutions can be experimentally probed using glass ion selective electrode methodologies if proper consideration is given to expected errors arising from competitive ion interference, liquid junction potential errors, and chemical attack of the sensor electrode. The feasibility of pH measurement of extremely concentrated alkaline solutions has been exemplified with potassium hydroxide electrolytes, and reproducible pH values can be measured with a room temperature stability of several hours. As shown in the inset of Figure 5, ion selective glass electrodes are also available which generate logarithmic response to activity of a variety of cations. Under controlled potentiometric conditions, using an approach analogous to the high pH measurements discussed in this paper, this can permit cation, determination in highly concentrated salt solutions, and has been applied to the potentiometric determination of potassium activities in highly concentrated potassium sulfide solutions as shown in Figure 5. These measurements indicated that the second acid dissociation constant of hydrogen sulfide was considerably smaller (by five orders of magnitude) than generally had been thought, and could only be measured in extremely concentrated electrolytes. This would substantially alter the solubility products of a wide variety of metal sulfides [18]. In order to verify this, other methods of concentrated electrolyte analysis were sought.

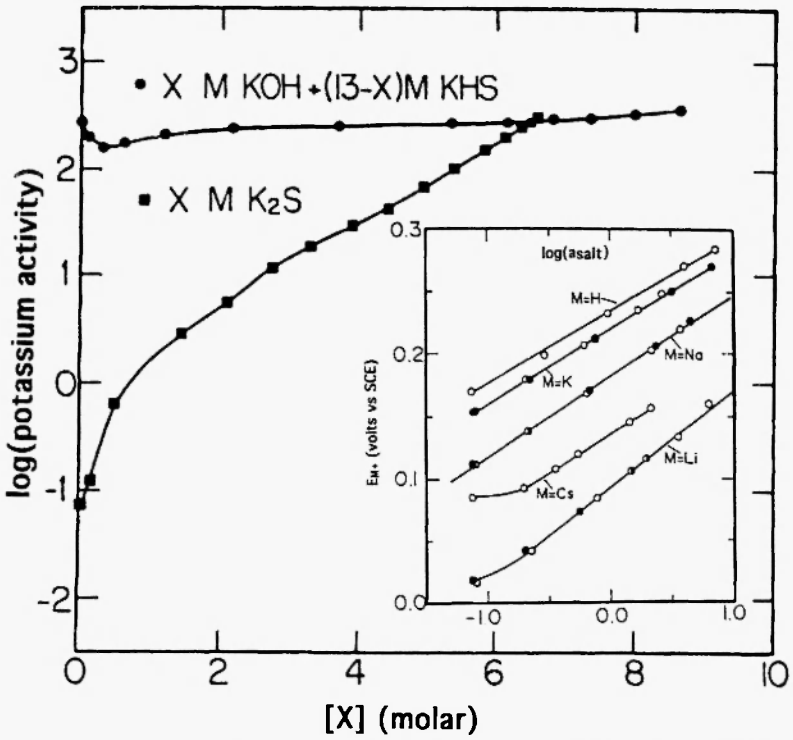

FIGURE 5 The measured potassium activity at 25°C of aqueous solutions X molar in either K_2S (lower curve) or in a solution containing a constant 13 molar concentration of K^+ in which 13 **M** KHS is titrated by 13 **M** KOH (upper curve). From reference 17. Inset: The voltage response of a Beckman 39137 cationic selective electrode, measured versus a Radiometer K401 saturated calomel electrode, in aqueous alkali chloride and hydroxide solutions at 25°C. Data for 0.1, 0.3, 1.0 and 4.5 **m** halide (open circle) and hydroxide (solid circle) solutions are generally presented. Due to solubility limitations, data for 4.0 **m** LiOH is presented, and an additional data point for 0.6 **m** CsCl is included. From reference 8.

III. EVANESCENT (SOLVENT) ACTIVITY ANALYSIS

A. Solvent Activity

Another approach to exploring the chemistry of concentrated solutions is to infer information regarding the chemical interactions of the solute species by measuring properties of the solvent. "Pure" solvent

(without added salt) has an activity of unity. In dilute solutions many bulk solvent properties are substantially unaffected by the dissolved salt. However, in increasingly concentrated solutions a growing fraction of the solvent will be directly influenced by solute/solvent interactions. For example as discussed in section II.C, in concentrated aqueous solutions the majority of the water can be strongly bound within the solvation sphere of ionic hydration and the water activity can drop by an order of magnitude. The number of water molecules associated with the hydration sphere of a dissolved ion varies by several fold depending on the experimental technique employed to make the measurement. However, several techniques indicate the primary hydration sphere surrounding Li^+, Na^+, K^+, and Cs^+ cations contain respectively approximately 9, 5, 3 and 0 water molecules. A concentrated solution can contain several moles of salt per 55.51 moles (1 kg) of water. Even these approximate values for alkali cation hydration sphere indicate that a substantial fraction of water in concentrated lithium, sodium or potassium salt solutions will be bound in hydration spheres. This is readily evident in the vapor pressure above these solutions which falls proportionally to the drop in water activity.

The water activity, a_w, of aqueous solutions, has been characterized and parameterized with a single coefficient, of α_o, for each specified salt expressing the variation of water activity with molal solution concentration, C. At a constant temperature, T, this results in the general expression [19]:

$$\alpha_o = - 127.8 \, (\partial \log a_w \, / \, \partial C)_T \qquad (12)$$

Table 2 lists the reported water activity values of a variety of saturated solutions at 25°C, and where available the values for α_o [19,20].

The theory of the inter-relationship of the solvent activity and the mean solution activity is well established and permits a mathematical vehicle to determine solute activity from measured solvent activity. In the next section, this theory is reviewed, and then in the following section an experimental methodology for the rapid determination of solvent activity will be presented.

B. Determination of Mean Solution Activity from Solvent Activity

Compared to the thermodynamic standard state of a pure solvent "s", $a_s^o \equiv 1$, the activity of the solvent component in an electrolytic solution, a_s, is given by:

$$a_s = \quad P_s \, / \, P_s^o \qquad (13)$$

TABLE 2. The variation of water activity, a_w , and also a_o (equation (12)), for saturated solutions in equilibrium at 25°C of the indicated salt (collated from references 8a and 8b).

salt	solubility, molal	α_o	a_w
none			1.000
K_2CrO_7	0.6		0.980
KNO_3	3.8	0.74	0.925
KBr	5.8	2.25	0.807
NaCl	6.2	3.45	0.753
$NaNO_7$	13.		0.65
NaBr	9.2	25.6	0.577
$Mg(NO_3)_2$	4.9	12.1	0.529
K_2CO_3	8.3		0.428
$MgCl_2$	5.9	20.9	0.330
$CaCl_2$	7.5	11.1	0.284
KOH	20.8		0.080

where P_s and P_s^o are the respective partial pressures (or more precisely the fugacity) for the solution or pure solvent. In a solution containing one or more electrolytes, k_1, k_2, k_3..., quantitative variations of solvent activity from unity, are emphasized by a parameter defined as the osmotic coefficient, φ:

$$\varphi = -1000 \ln a_s / M_s (\sum_k n_k m_k) \quad (14)$$

where M_s is the molar mass of the solvent, and one mole of electrolyte gives ν_k moles of ions in solution.

A precise knowledge of solvent activity, such as a_w for aqueous solutions, reveals direct information of a variety of physical chemical properties including osmotic pressure, freezing point depression and boiling point elevation. Additionally Gibbs, Duhem and others, have shown that each of the activity coefficients of a multicomponent system may be calculated given the activity coefficient variation of any one component as a function of system composition [21a]. Hence, mean solution and solute activity may be determined from solvent activity when this solvent activity has been determined over a wide electrolyte concentration range. In concentrated electrolytes, the mass fraction or molal fraction of solute becomes significant compared to that of the solvent. In this case, a method to monitor solvent activity may reveal significant variations in electrolyte speciation.

In aqueous solution a_w, solvent activity, is often summarized by osmotic coefficient from equation (14):

$$\varphi = -55.51 \ln a_w / (\Sigma_k \nu_k m_k) \quad (15)$$

In accordance with Gibbs and Duhem, the mean solution activity, $\gamma_\pm$, is intimately related to φ (and therefore solvent activity), and at a given concentration, C [21a]:

$$\ln \gamma_\pm(m) = \varphi(m) - 1 + \int_{c=0}^{m} [\varphi(C) - 1] C^{-1} d \quad (16)$$

Solute activity may be determined from equations (15) and (16), when solvent activity have been determined over a wide concentration range of electrolyte. Inversely the osmotic coefficient and therefore the water activity, may be determined when the mean solution activity is known:

$$\varphi(m) = 1 + m^{-1} \int_{c=0}^{m} C \, d \ln \gamma_\pm(C) \quad (17)$$

C. Traditional Analysis of Activity

In 1917 Bousfield introduced the concept of "isopiestic solutions" to determine the concentrations of solutions having the same vapor pressure [22]. In isopiestic methods two open solutions, one of known solvent activity and the other of unknown solvent activity, are placed in an enclosed container which permits free solvent exchange between the solutions. The solutions are allowed to come to thermal equilibrium resulting in a fixed vapor pressure in the container. During this equilibration process there is a mass gain or loss from the known solution during the condensation or distillation from the unknown solution. This mass change is then measured and related to solvent activity of the known solution. This process may be iterated until the solvent activity in the unknown solution is determined by choice of a known solution which undergoes no mass change and therefore no net solvent exchange. Isopiestic methods were modified several times in the early 1900s, and used extensively in the first half of this century. However, these method requires on the order of days for a single measurement [23-25].

Electrolyte activities may be determined by any method that either directly or indirectly probes the chemical potential of solvent or

solute in solution. These methods include isopiestic [21b], potentiometric [21c], freezing point, boiling point, osmotic pressure, relative speciation, solubility, and transport properties including conductivity and diffusion [21d]. The solvent and mean solution activities of several hundred single-salt solutions have been determined. Of these the majority have been studied by the isopiestic method [21d,23-27] which is also more applicable for highly speciated equilibria, in which potentiometric (Nernstian) analysis would be complex or not suitable [21c]. We therefore sought a contemporary methodology to speed up the lengthy measurement time required for traditional isopiestic methods. This method has been termed "evanescent" (evanescent ≡ transitory, dissipating like a vapor), and is discussed in the following section.

D. Evanescent Methodology for Analysis of Solvent Activity

Evanescence methodology digitally monitors the real time mass variation of a solution to determine the rate of driven evaporative loss as a function of time in a controlled environment. In this method, the dynamic mass loss via solvent evaporation, dm_{soln}/dt, from the liquid phase can be used as a probe to determine solvent activity to a high degree of precision. At constant temperature, the evaporation rate of solvent from solution will be related to the differential of the solvent partial pressure in the ambient gas phase and the thermodynamic partial pressure limited by the solvent activity in solution. In this method of analysis, the partial pressure of solvent in the ambient gas is effectively kept fixed and the resultant dynamic mass loss is monitored and related to solvent activity. The effect leads to solvent activity measurements accelerated compared to previous conventional isopiestic measurements. This is accomplished by introducing a reproducible gas boundary layer consisting of a relatively non-turbulent regulated flow of gas across a fixed geometry of the solution under analysis. The gas is introduced with a fixed partial pressure of solvent, and the time variation of the resultant solution mass is monitored. Differential solution mass, dm_{soln}/dt, is calculated in real time and related to calibrated $dm_{standard}/dt$ for solutions of known activity, resulting in determination of sample solvent activity.

Evanescent solvent activity applied to the determination of water activity is summarized in the top left of Figure 6. Highly dried gas, such as argon passed over a dessicator, is introduced at fixed temperature and flow rate into a confined electroanalytical balance chamber. In the chamber, the gas flows over a "Test Solution", the analyte solution, at a flow rate optimized to maximize solution evaporation without inducing excessive solution turbulence. The rate of

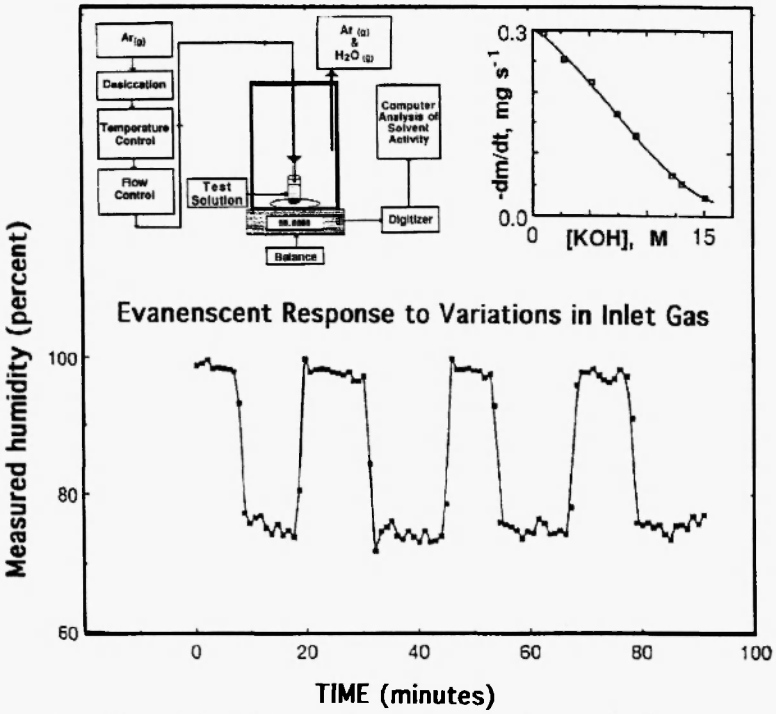

FIGURE 6 Top left: Schematic representation of the evanescent determination of solvent activity for a "Test Solution". An on-line computer compares the rate of solvent loss to calibrated evanescent loss of solutions of known solvent activity, and converts the digitized mass variation to solvent activity of the Test Solution. In the evanescent solvent activity apparatus used, all control gases were initially dehydrated and temperature controlled to 25 ± 0.3°C by passing through an extended stainless steel tubular coil immersed in a 25°C water bath. Output gas flow rate, typically maintained at 25 cm^3/second, was controlled by valve and monitored using a conventional Fisher Scientific Precision bore flowrator 01-150/S-51801 flow meter. Mass measurements were determined with a Fischer XA-200 electroanalytical balance with 0.1 mg resolution. The balance, interfaced through an RS-232C serial port, internally accumulates and digitizes measured mass every 2.5 seconds. TRUE BASIC software was developed to create algorithms for on-line mass collection, the calculation of differential mass, and analysis of solvent activity. Figure bottom: The time response of evanescent analysis. Evanescent measurement conducted using a fixed sample solution, in which the inlet gas is not dry argon, but rather cycled between argon fixed with either 100% or 75% relatively humidity at 25.0°C. Figure inset, top right : evanescent time evolved rate of mass loss, dm/dt, as a function of KOH molar solution concentration.

evaporation of solvent from the Test Solution is monitored as mass loss by the electroanalytical balance, digitized and interfaced to a computer which continuously determines differential mass loss as a function of time. The differential mass is compared to the mass loss induced from standard solutions of known solvent activity and converted to solvent activity of the Test Solution. As exemplified in Figure 6, in which the inlet gas humidity is varied, the time response for evanescent analysis is on the order of minutes, rather than the time scale of days associated with conventional isopiestic measurement.

Evanescent activity measurements were examined by bringing argon in contact with a variety of standard solutions of known solvent activity. Evanescent calibration with KOH standard solutions is described herein. Further experimental results summarizing evanescent measurements in a variety of different salt solutions are found in references 3 and 28. Figure 7 presents the evanescent mass loss of a variety of concentrated aqueous KOH test solutions at 25°C. From the data in this figure, the inset in the top right of Figure 6 summarizes the measured value of $dmass_{soln}/dt$ as a function of KOH solution concentration. Under a fixed gas flow and fixed cell geometry conditions, the mass transport rate of solvent across the gas/liquid interface, $dmass_{soln}/dt$, is related to the differential between the solution solvent activity and the solvent partial pressure in the flow gas, p_w:

$$dmass_{soln}/dt \propto a_w - p_w \quad (18)$$

There are limits to which the rate, $dmass_{soln}/dt$, will remain proportional to the solvent activity. Limiting the choice of analytes to nonvolatile solutes, including most conventional salts in aqueous solution, constrains the solution's mass variation to solvent, and simplifies interpretation of $dmass_{soln}/dt$. From a thermodynamic perspective, the ideal case occurs at $dmass_{soln}/dt = 0$. In this case, when the flow gas contains a solvent content, p_w, equivalent to the solution's solvent activity, no net exchange of solvent occurs across the solution/gas interface, and equilibrium activities are probed. Equilibrium is also approached as the gas flow rates approaches zero. The system then has infinite time to equilibrate the gas partial pressure to the solvent activity. At higher flow rates, a kinetic process (evaporative losses) is being used to probe thermodyanic information (solvent activity), and flow conditions will perturb the system from equilibria. In particular the enthalpy of vaporization of most solutions is significant, and cooling due to evaporation will perturb the solution activity. At room temperature, each °C increases the vapor pressure of water by 8%. From a practical perspective, during measurement the gas flow rate is kept low to insure the solution temperature is effected by less than 0.1 °C.

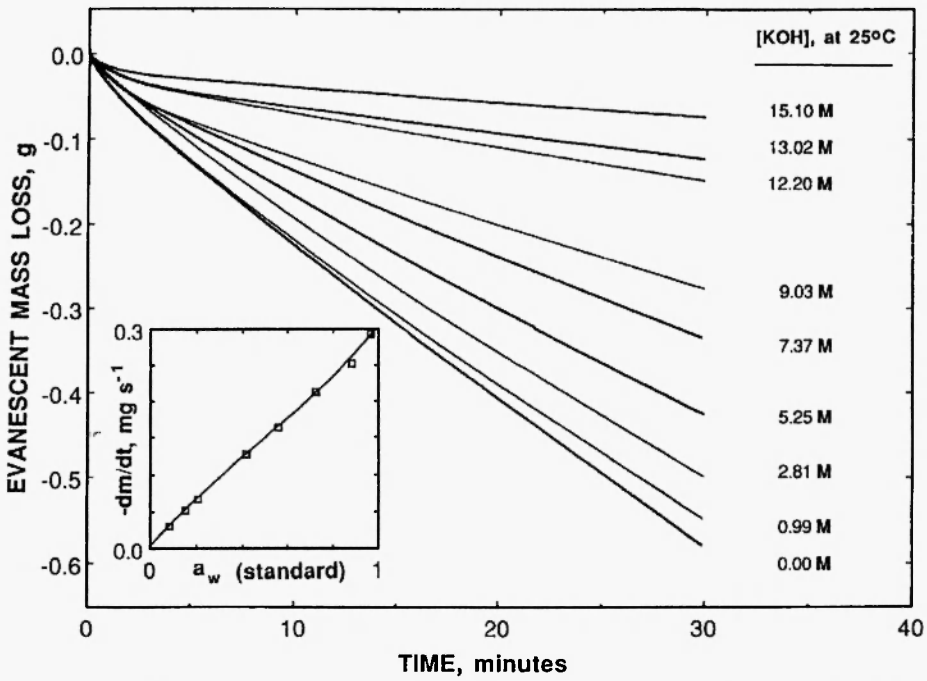

FIGURE 7 The evanescent mass loss of solvent from a variety of aqueous KOH solutions. Evaporation of solvent from each KOH solution to desiccated Ar_{gas} is monitored by the mass loss of water at 25.0°C, using the experimental configuration described in the Figure 6 legend and as further described in references 3 and 28. Inset: The variation of solvent mass loss, -dm/dt , with known water activity in aqueous KOH solutions. The curve represents a best third order polynomial fit of the data.

The linear response of the evanescent technique to probe a range of solvent activity is demonstrated with well characterized KOH solutions (Tables 1 and 2). The variations of these known (standard) water activities as a function of measured evanescent solvent loss, $dmass_{soln}/dt$, is summarized in the inset of Figure 7. In accordance with equation (18), the variation of $dmass_{soln}/dt$ with a_w is highly linear to a first-order approximation, but small deviations to linearity are observed at both the low-and high-solvent activity extremes. Deviations may occur with imperfect temperature control, initial residual solvent in the carrier gas, or turbulence at the gas/liquid interface. Compensations for small deviations from linearity are incorporated by fitting a third-order polynomial for a_w. The resultant polynomial acts as a calibrating standard, an algorithm for on-line conversion of measured dmass/dt to

solvent activity. This method provides a measurement of water activities in Figure 8 to an average reproducibility of 1.0% over the activity range varying from 0.86 to 0.20, and 1.6% over the full 0 - 1.0 a_w range.

Figure 9 summarizes solutions mass losses, $dmass_{soln}/dt$, from aqueous K_2S solutions at 25°C over a wide concentration range. Potassium sulfide solutions may be nominally described as either K_2S solutions or as solutions equimolar in KOH and KHS. Molal and molar concentrations of equivalent solutions are presented in the first two columns of Table 3 and are consistent with recent density determinations [1]. The measured value of solvent mass loss, $dmass_{soln}/dt$, was determined for each of the K_2S solutions as a function of solution molarity. The direct conversion of dmass/dt to a_w for K_2S is quantified in the calibration presented in the inset of Figure 7. The resulting analyzed values of a_w for aqueous K_2S solutions are presented in column 3 of Table 3.

Solution osmotic coefficients for sulfide solutions, φ, are presented in column 5 of Table 3 as determined from equation (15) using the evanescent

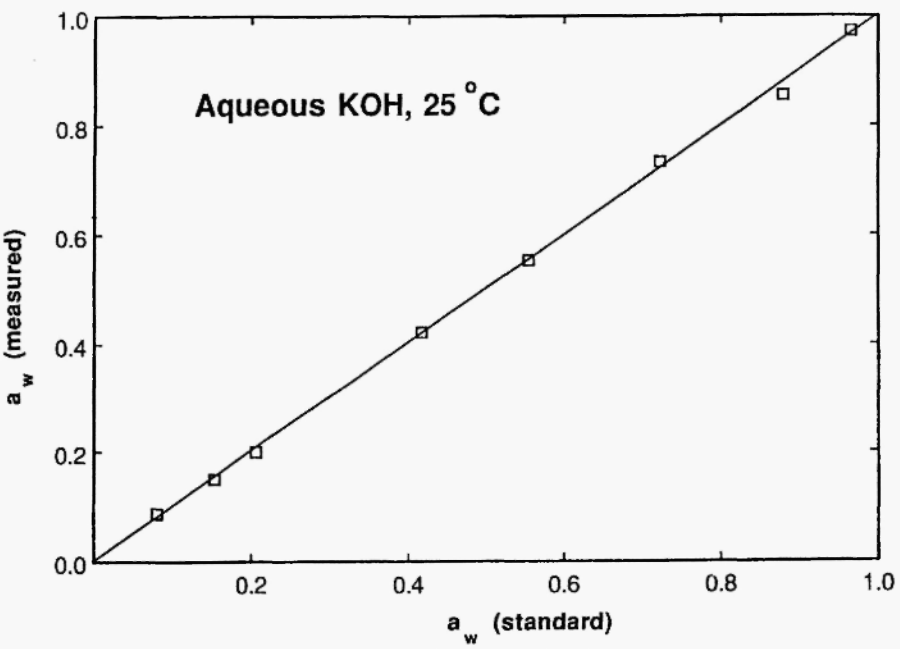

FIGURE 8 Comparison of known (standard) solvent activities in aqueous KOH solutions with those regenerated from evanescent measurements at 25°C. Values for measured activity are determined from measured evanescent values of dm/dt using a third order polynomial fit of dm/dt versus a_w data summarized in the figure inset.

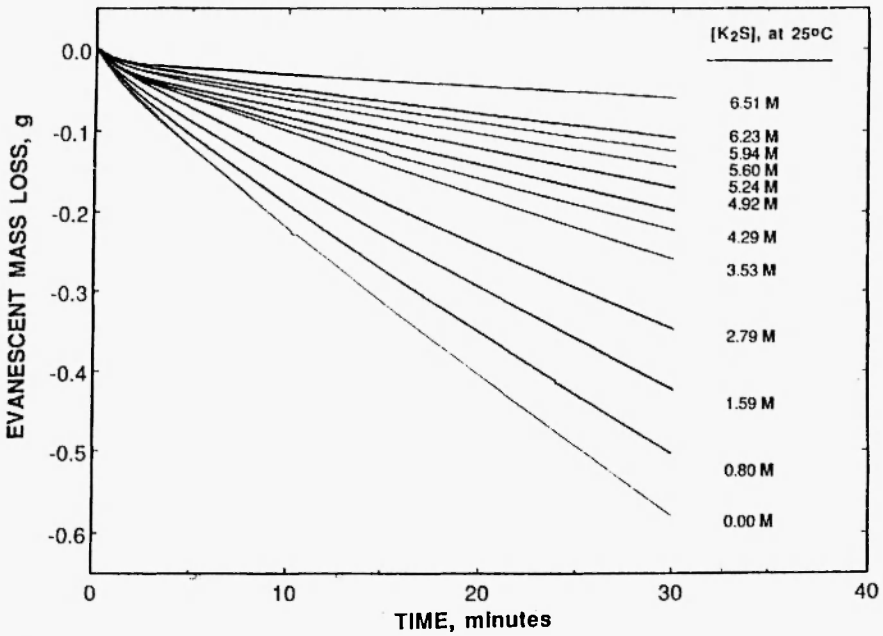

FIGURE 9 The evanescent mass loss of solvent from a variety of aqueous K_2S solutions. Evaporation of solvent from each K_2S solution is monitored by the mass loss of water at 25.0°C, using the experimental configuration described in the Figure 9 legend and in reference 28.

TABLE 3. Solvent and mean solution activities of aqueous potassium sulfide solutions at 25°C. a_w is measured using the evanescent technique as described in the text. φ and $\gamma_{\pm}$ are calculated in accordance with equation (15) and (16).

$[K^+]$, molar	$[K^+]$, molal	a_w,	$a_{\pm}$,	φ	$\gamma_{\pm}$
0.00	0.00	1.00	0.00	--	1.00
0.99	1.01	0.96	0.76	0.99	0.76
1.60	1.65	0.95	1.17	0.95	0.71
3.18	3.44	0.86	3.20	1.20	0.93
5.58	6.50	0.73	8.51	1.37	1.31
7.06	8.65	0.59	18.2	1.69	2.10
9.21	12.3	0.41	47.8	2.01	3.89
10.5	14.8	0.32	79.1	2.13	5.34
11.2	16.4	0.28	103.	2.18	6.29
11.9	17.9	0.23	135	2.24	7.50
12.5	19.4	0.20	170.	2.30	8.75
13.0	20.9	0.17	211.	2.34	10.1

water activities summarized in column 3 of this table. Substitution of these osmotic coefficients into equation (15), and a conventional trapezoidal integration of the concentration variation of equation (16), results in the mean molal activity coefficient summarized in column 6 of Table 3. From these values in the high alkaline sulfide concentration domain, the evanescent technique provides in column 4 the first measurements for mean solution activity in sulfide solution, $a_{\pm}$, pertinent to an understanding of the sulfide second acid dissociation constant which are summarized. As seen in this column, and analogous to concentrated potassium hydroxide solutions, very high solution activities dominate in this high concentration domain [3].

The evanescent (driven evaporation) technique provides a contemporary method to probe and broaden the understanding of solvent activity in concentrated electrolyte. The measured values of solvent activity provide analyte information by determination of solution activity in accordance with equations (15) and (16). The methodology determines the rate of driven evaporative loss as a function of time in a controlled environment, and evaporation rate correlates with solvent activity for a wide variety of known solutions. As opposed to conventional isopiestic methods, which can take days to determine solvent activity and are therefore often not useful in highly unstable, volatile, caustic or reactive media evanescent methodology is demonstrated to determine solvent activity within minutes to a precision of better than 2 percent.

IV. CONDUCTOMETRIC ANALYSIS OF CONCENTRATED SOLUTIONS

A. Conventional Conductometric Titration

Two general instrumental techniques have been utilized for conductometric analysis of solutions. The first, common to academic and environmental laboratory, immerses two electrodes of fixed geometry in solution. An alternating potential is applied, at the electrodes and the solution conductance component portion of the impedance signal is electronically determined. The second technique, often found in industrial applications, is electrodeless conductivity in which torroidal electrodes are situated on each side, but external, to the solution being investigated. An oscillating potential is applied to the first and induced in the second torroid, and the solution conductance is determined [29]. A variety of calibrating solutions have been determined for analysis of solution conductance [30].

Conductometric analytical methodologies make use of the different specific conductance of ions to determine which species are present in solution. These methodologies are particularly suitable for distinguishing between covalent, single and multiple charge species, between soluble and insoluble species (as in solubility product determination), and acid dissociation constants. In aqueous media the hydrogen ion and hydroxide ion mobilities are several fold higher than all other ions [31], and reflect the unique hopping/tunneling conductance mechanisms available to only H^+ or OH^- ion/solvent interactions. Therefore, conductometric measurement of H^+ or OH^- during acid/base titration presents an easily discerned and widely used indicator to probe the degree of acid protonation in muliprotonic acid; as in our study of ferrocyanic and ferricyanic acid [32]. The equivalent conductivity of hydrogen ion and hydroxide ion are presented in Table 4 for water from the melting through critical points.

B. Conventional Conductometric Titration of Concentrated Solution

Conductometric titrations conventionally utilize a titrant substantially more concentrated than the analyte, with the equivalence point and equilibrium constant related to the derivative of the conductivity variation. When this is not feasible, as in the study of highly concentrated analytes, an equally valid approach is to use equimolar (equally concentrated) analyte and titrant solutions, and to model the results to expected conductance variation for the equilibrium under consideration. An example of this approach is presented here in which the high mobility of hydroxide is utilized to probe the extent of free hydroxide in KHS solution to probe the second acid dissociation constant, $\mathbf{K_2}$, of H_2S. If during the course of the titration added hydroxide does not react, then solution conductance is expected to rise. However, this will not be the case if added OH^- reacts with free HS^- according to the hydrolysis reaction associated with $\mathbf{K_2}$:

$$HS^- + OH^- \rightleftarrows H_2O + S^{2-}; \quad \mathbf{K_{2b'}} = \mathbf{K_2 / K_w} = \frac{a_w \, a_{S^{2-}}}{a_{HS^-} \, a_{OH^-}} \qquad (19)$$

Figure 10 summarizes the measured conductometric titration of 6.5, 9.5 or 12.83 molar KHS solutions during titration by equimolar (respectively 6.5, 9.5 or 12.83 M) KOH solutions at 25°C. The figure inset presents two idealized variations of titrated KHS with added KOH, as the solution conductivity varies from that of the pure KHS electrolyte. The dotted curve in Figure 10 inset indicates the expected variation in conductivity if there is no interaction between hydrosulfide and

TABLE 4. The equivalent conductivity of hydrogen ion and hydroxide ion in water. From T. S. Light, S. Licht, "Conductivity and Resistivity of Water From The Melting Through Critical Points"*Anal. Chem., 59,* 2327 (1987).

temp, °C	pK_w	λ, $cm^2\ \Omega^{-1}\ equiv^{-1}$		
		$\lambda^{\circ}H^+$	$\lambda^{\circ}OH^-$	$\lambda^{\circ}H^+ + \lambda^{\circ}OH^-$
0	14.938	224.1	117.8	341.9
5	14.727	250.0	133.6	383.6
10	14.528	275.6	149.6	425.2
15	14.340	300.9	165.9	466.8
18	14.233	315.8	175.8	491.6
20	14.163	325.7	182.5	508.2
25	13.995	350.1	199.2	549.3
30	13.836	374.0	216.1	590.1
35	13.685	397.4	233.0	630.4
40	13.542	420.0	250.1	670.1
45	13.405	442.0	267.2	709.2
50	13.275	463.3	284.3	747.6
55	13.152	483.8	301.4	785.2
60	13.034	503.4	318.5	821.9
65	12.921	522.0	335.4	857.4
70	12.814	539.7	352.2	891.9
75	12.711	556.4	368.8	925.2
80	12.613	572.0	385.2	957.2
85	12.520	586.4	401.4	987.8
90	12.431	599.6	417.3	1017
95	12.345	611.6	432.8	1044
100	12.264	622.2	448.1	1070
125	11.911			1196
150	11.637			1323
175	11.431			1425
200	11.288	824	701	1525
225	11.207			1581
250	11.192			1636
275	11.251			1676
300	11.406	894	821	1715
325	11.705			1737
350	12.295			1759
374	15.641			1780

hydroxide. Hence, as seen at 50 percent added KOH, the conductivity acts as the simple average of the KHS and the higher KOH solution conductivities. In the second situation, the dashed curve in the figure inset indicates the expected variation in conductivity if the interaction of each hydrosulfide and hydroxide reacts fully to produce a free sulfide.

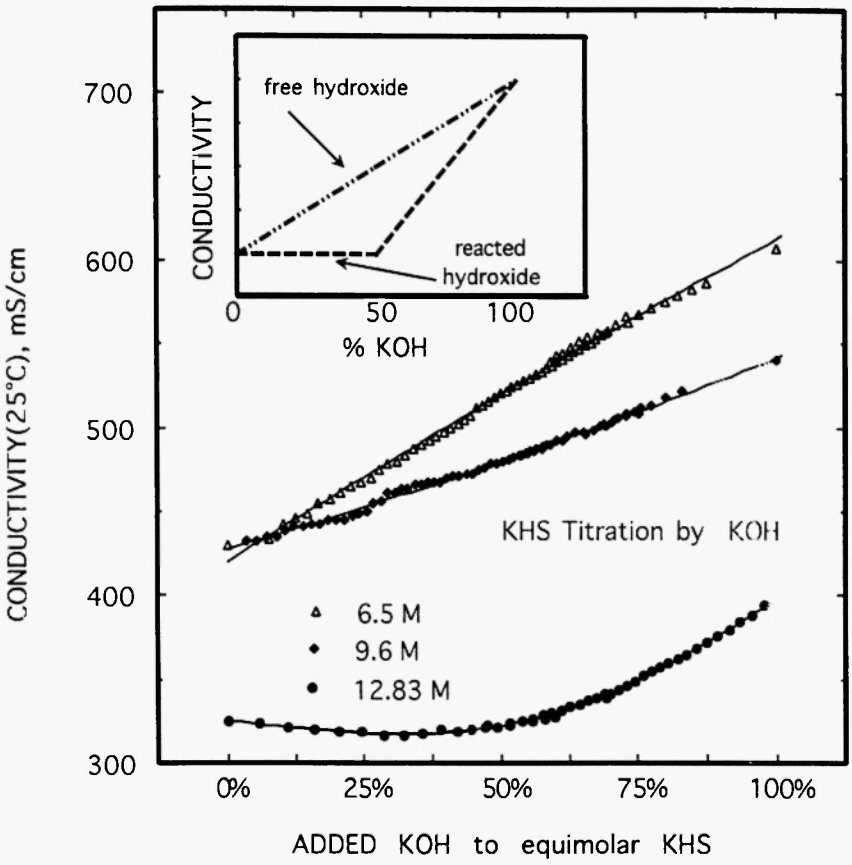

FIGURE 10 The measured conductivity of 6.5, 9.5 or 12.83 M KHS solutions during titration by equimolar (respectively 6.5, 9.5 or 12.83 M) KOH solutions at 25°C. Inset: the dotted curve indicates the expected variation in conductivity if the interaction of hydrosulfide and hydroxide produces no free sulfide; the dashed curve indicates the expected variation in conductivity if the interaction of each hydrosulfide and hydroxide reacts fully to produce a free sulfide, and assumes sulfide equivalent conductivity approximates hydrosulfide equivalent conductivity. Electrolytic conductivity was measured with a YSI 35 conductance meter and a Balsbaugh conductance probe with a cell constant of 10 cm^{-1}. The probe has a Noryl body and graphite electrodes minimizing both alkali attack and sulfide poisoning of the electrodes. The probe was calibrated with 1.00 M KCl solutions. Further experimental details are presented in reference 32.

In this situation, the point of 50 percent added KOH reflects a solution containing only K_2S, and cannot contain the highly mobile hydroxide species. Each free sulfide is assumed to have equivalent conductivity substantially less than that of hydroxide and approximately that of free hydrosulfide.

In Figure 10, the measured conductivity variation in the titration of KHS by KOH can be compared to the expected variation, as shown in the inset. In the 6.5 and 9.5 **M** titrations, the linear increase in conductivity with increasing KOH provides substantial evidence that added OH^- remains unassociated, and there is little free sulfide in solution. However, the observed similarity of the 12.83 **M** titration curve to the dashed curve in Figure 10, indicates diminished free hydroxide in this solution and the formation of substantial quantities of free sulfide. The extent of these variations can be quantified by calculation of the distribution of species in solution as a function of the extent of titration, and reflect that little free S^{2-} exists in all but the most concentrated alkaline environments, expressed by the second acid dissociation constant of approximately $\mathbf{K_2} = 10^{-17}$. However, more precise measurements of $\mathbf{K_2}$ can be determined using the differential conductometric methodology presented in the next section.

C. Differential Conductometric Methodology

Differential conductometric analysis compares the specific conductances of isolated and equilibrated phases in liquid phase systems [33]. In concentrated solutions containing reagents A and B, the specific conductance change should act as a probe to gauge the equilibrium distribution of species in solution. The differential conductance, $\Delta\sigma_P$, measures the difference in the specific conductance of solutions containing the isolated reactants, σ_A and σ_B, compared to the specific conductance in the equilibrated system, σ_P, described in the equilibrium:

$$A + B \rightleftarrows P \qquad (20)$$

The differential conductance varies as a function of the given concentration, C, of isolated or combined equilibrated reactants:

$$\Delta\sigma_P(C) = 0.5(\sigma_A(C) + \sigma_B(C)) - \sigma_P(C) \qquad (21)$$

D. An Example of Differential Conductometric Methodology,

The variation of aqueous KOH, KHS and K_2S specific conductance at 25°C, and over a wide range of concentrations, is presented

in Figure 11. K^+ and HS^- have comparable limiting equivalent conductances ($\lambda^o_{K^+}$ = 74 S cm^2 equiv^{-1} and $\lambda^o_{HS^-}$ = 67 S cm^2 equiv^{-1} respectively at 25°C). The KOH specific conductance is dominated by the exceptionally high equivalent conductance of hydroxide, $\lambda^o_{OH^-}$ = 199 S cm^2 equiv^{-1} at 25°C.

In Figure 12, the magnitude of the σ_{K_2S} deviation is reported as a differential conductance, $\Delta\sigma_{K_2S}$, determined as:

$$\Delta\sigma_{K_2S} = 0.5(\sigma_{KHS} + \sigma_{KOH}) - \sigma_{K_2S} \quad (22)$$

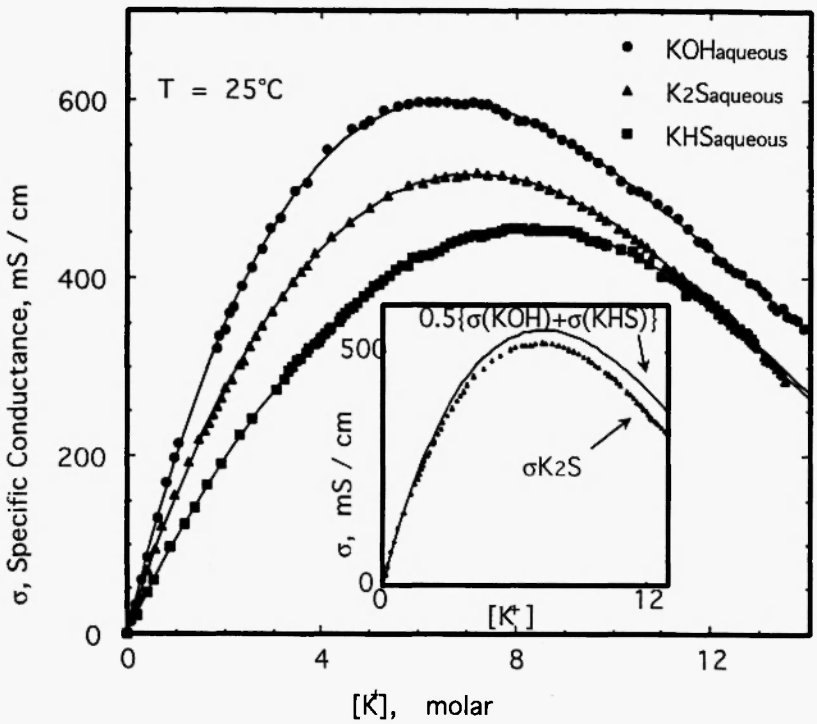

FIGURE 11 The conductivity of concentrated KOH, K_2S or KHS aqueous electrolytes at 25°C. $[K^+]$ refers to the molar concentration of K^+ in an aqueous solution containing only the potassium salt indicated. Further details are presented in reference 32. Inset: aqueous K_2S conductivity compared to the average of the KHS and KOH conductivity as a function of concentration. $0.5(\sigma_{KHS} + \sigma_{KOH})$, is determined by a fifth order polynomial fit of experimental conductivity, as summarized in Table II.

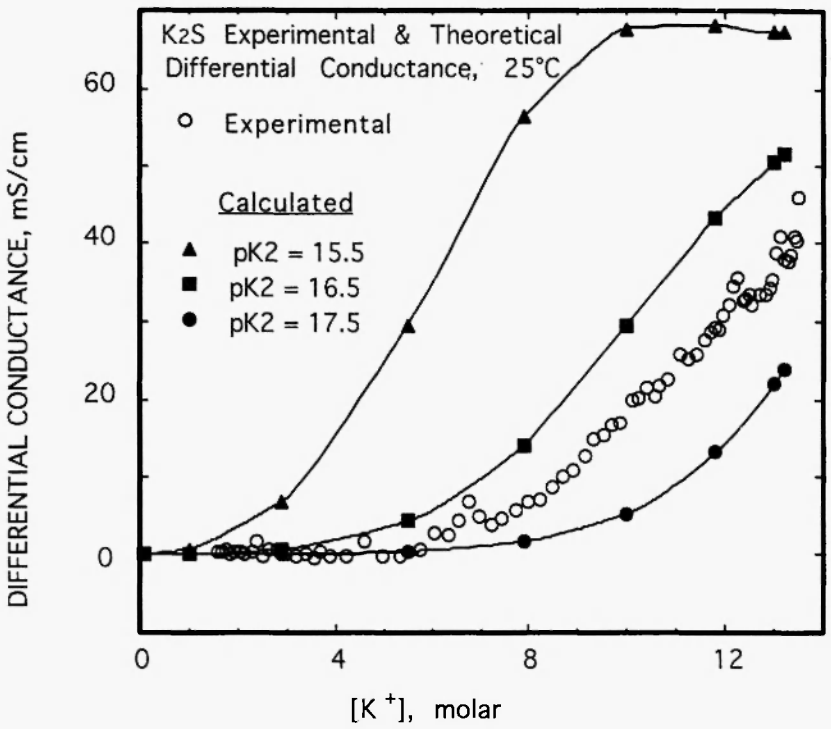

FIGURE 12 Predicted and experimental differential conductivity, $0.5(\sigma_{KHS} + \sigma_{KOH}) - \sigma_{K_2S}$, of aqueous K_2S solutions at 25°C. Differential conductivity is determined as the magnitude of the K_2S conductivity deviation from the average of the KHS and KOH conductivities. The nominal molar concentration of each solution may be described as $[K_2S] = 0.5[K^+]$ or alternatively as a solution comprised of $[KHS] = [K^+]$ and $[KOH] = [K^+]$. Predicted differential conductivity for K_2S is calculated from equations (22), using the relative distribution of ions in solution, equations (19), and utilizes the experimental conductivities of equivalent KOH and KHS solutions.

The variation of the aqueous potassium sulfide specific conductance, σ_{K_2S}, can be separated into two distinct regions when compared to KHS and KOH electrolytes of similar concentration. As shown by the differential conductance measurements reported in Figure 12, aqueous K_2S electrolytes containing less than 6 **M** K^+ act in a manner similar to an average of equimolar separate solutions of KOH and KHS.

This variation in conductance reflects the distribution of species within these solutions. At sufficiently low concentrations of K_2S, there is virtually complete hydrolysis, no free sulfide exists, and these electrolytes act as simple solutions containing equimolar free OH^- and HS^-, in accordance with the left side of equation (19). These conditions can be only be met for a second acid dissociation constant of H_2S which is several orders of magnitude smaller than commonly reported.

In aqueous K_2S electrolytes containing greater than 6 **M** K^+, the increase in differential conductance parallels the depletion of free OH^- and the formation of free S^{2-}. Figure 12 compares predicted and experimental differential conductivity of aqueous K_2S solutions at 25°C. $\mathbf{K_2}$ on the order of 10^{-12}, as had been reported, would lead to a much sharper rise in differential conductance than observed. In Figure 12 the predicted differential conductance for K_2S are calculated based on $\mathbf{K_2}$ values varying from $10^{-15.5}$ to $10^{-17.5}$. A best fit of $p\mathbf{K_2} = 16.9 \pm 0.2$ models the measured differential conductance for the complete range of K_2S concentrations studied [33].

V. DIFFERENTIAL DENSOMETRIC ANALYSIS

A. Differential Densometric Principles

In dilute solutions, the molecular volume change associated with chemical reactions, has little affect on the density of the bulk solution. However in concentrated solutions, the solute constitutes a significant fraction of the solution, and changes in molecular volume change associated with chemical reactions will be reflected by significant changes in the density of the bulk solution.

The combined volume of the solute in concentrated electrolytes can be significant compared to the total solvent volume. Indeed, the volume encompassed by dissolved hydrated species in approximately 10 **M** aqueous salt solutions can be larger than that encompassed by the volume of free water. The combined volume of individual solute species may be substantially affected by equilibrium displacement, including that occurring by simple addition, as exemplified by equation (20) or by charge transfer: from reactants A, B to form products C, D:

$$A^- + B^- \rightleftarrows C^{2-} + D \qquad (23)$$

Differential densometric analysis compares the densities of isolated and equilibrated phases in a system. Figure 13 illustrates the variation in volume which can occur between such isolated and equilibrated phases in a system. In concentrated solutions of reactants A

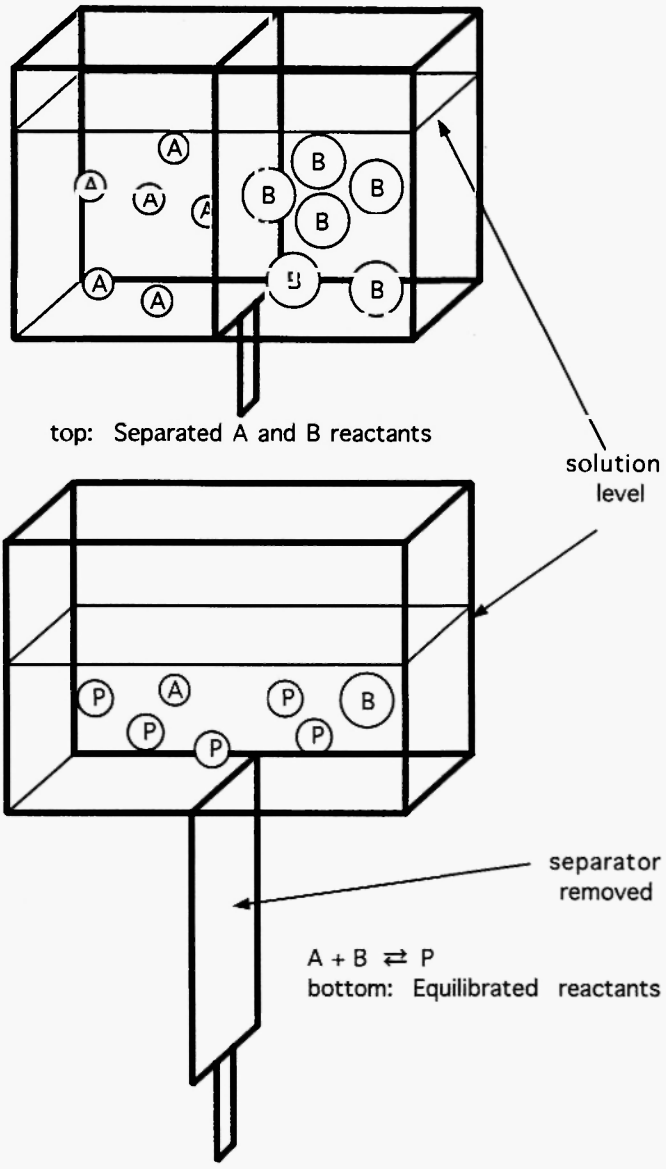

FIGURE 13 Schematic of decrease in bulk solution volume occurring when the molecular volume of product species, P, is smaller than the combined molecular volumes of reactants A and B.

and B, the cumulative volume change should act as a probe to gauge the equilibrium distribution of species in solution. The differential density, $\Delta d_{A,B}$, measures the difference in the density of solutions containing the isolated reactants, d_A and d_B, compared to the density in the equilibrated system, $d_{A,B}$. The differential density varies as a function of the given concentration, C, of isolated or combined equilibrated reactants:

$$\Delta d_{A,B}(C) = d_{A,B}(C) - 0.5(d_A(C) + d_B(C)) \quad (24)$$

$\Delta d_{A,B}$ varies with the relative solvated volume of product and reactant species, and is proportional to the distribution of ions in solution. The concentration variation of $\Delta d_{A,B}(C)$ compared to that at a fixed concentration, $Dd_{A,B}(C_{fixed})$, acts as a measure of the relative concentration of products in these electrolytes. Hence in accordance with equations (20) and (23), for a solution that contains a total concentration, C = [A] + [B] + [P]:

$$\frac{[P]/C}{[P]_{fixed}/C_{fixed}} \cong \frac{\Delta d_{A,B}(C)}{d_{A,B}(C_{fixed}) - 0.5(d_A(C_{fixed}) + d_B(C_{fixed}))} \quad (25)$$

equation (24) becomes exact in the limit in which $[P]_{fixed}$ approaches C_{fixed}, i.e. complete reaction of A and B.

B. Differential Densometric Methodology

Differential densometric analysis requires precise measurement of differences in solution density. Specific gravity is readily measured by a Westphal balance in which the solution to be analyzed is situated on a balance; a plummet is suspended into the solution, displacing a fixed volume. The resultant measured mass change, is to relative specific gravity. The solution However, commercially available hydrometers and Westphal balances did not exhibit a desired relative density resolution of better than 0.0005 g/cm^3.

Specific gravity was measured with a contemporary in-house built Westphal balance, utilizing a ~15 cm^3 glass plummet externally suspended into a cell situated on a Fisher XA-200 0.0001g resolution electroanalytical balance RS-232C interfaced to a 8086 microcomputer. Specific gravity was measured by the loss in weight of the glass plummet brought about by its buoyant suspension in approximately 45 cc of the liquid to be measured. The cell was maintained at a constant temperature of 25.0±0.3°C, and the plummet was repeatedly calibrated upon

immersion in deionized distilled water. In water, the ratio of the ±0.0003g accuracy of the balance compared to the plummet mass yields a theoretical specific gravity reproducibility of 1.00000±0.00002. Temperature uncertainty in the specific gravity is comparable to a theoretical specific gravity resolution for water of 1.00000+0.00008. Actual reproducibility of the measured specific gravity was better than 1.0000±0.0002.

In this study, differential densometric analysis is defined in terms of molar concentration units. The variation of density and molarity are both related by the spatial constraints of the solution; whereas molality is constrained by solvent mass. Similarly, the hydrolysis reaction, equation (19), is a molar consistent, molal inconsistent, equation (as it involves solvent reaction). However, the required precision of the density measurements in this study dictated that molal concentrations be employed. Molar concentrations were subsequently determined from the solution density, d (for a solution comprised of a pure salt of molecular weight, W, the molarity = $d / (\text{molality}^{-1} + 0.001 \cdot W)$).

C. Differential Densometric Analysis Example

As discussed in Section III, a K_2S solution can be considered a combined equimolar solution of KOH and KHS. The concentration of HS^-, OH^- and S^{2-} in such solutions is constrained as equilibrium equation (19). The variation of aqueous KOH, KHS or K_2S specific gravity at 25°C, and over a wide range of molal concentrations, is presented in Figure 14. The specific gravity was determined relative to unity specific gravity at infinite dilution, i. e. the specific gravity$_{25°C}(H_2O) = 1$. The density is determined compared to the known density of water, i. e. $d_{25°C}(H_2O) = 0.99702\ g/cm^3$, and the resultant molar variation of density is presented in the inset of Figure 14. As seen in this figure, the functional variation of density is substantially linear with changes in concentration. A closer inspection of the (significant) contributions from higher order terms in the concentration variation of the density is achieved by first removing this large linear concentration dependence. This is derived by defining an equivalent density, scaled by concentration and similar to the concept of an equivalent conductance:

$$\text{equivalent density} = C^{-1}\{d(C) - d_{25°C}(H_2O)\} \qquad (26)$$

where C is the concentration of K^+ in gram equivalents per liter. Figure 14 inset presents the variation of KOH, KHS or K_2S equivalent density with concentration.

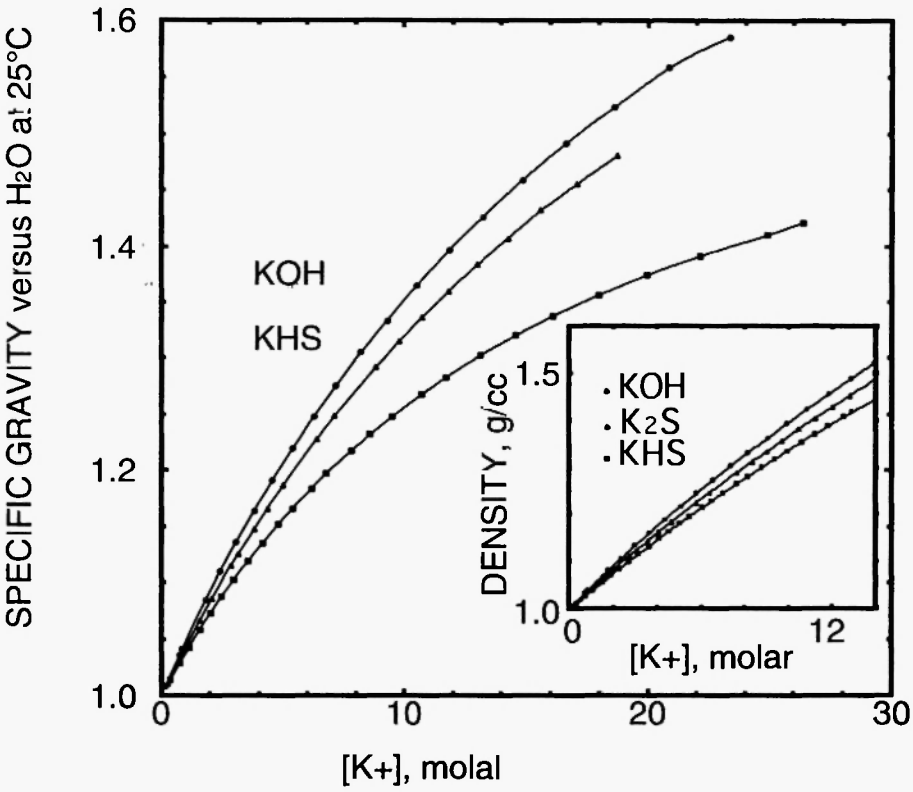

FIGURE 14 The measured specific gravity of concentrated KOH, K_2S or KHS aqueous electrolytes at 25°C. m_{K^+} refers to the **molal** concentration of K^+ in an aqueous solution containing only the potassium salt indicated. Inset: The density of concentrated KOH, K_2S or KHS aqueous electrolytes at 25°C. $[K^+]$ refers to the **molar** concentration of K^+ in an aqueous solution containing only the potassium salt indicated.

In accordance with equations 19 and 23, the differential density of a K_2S solution is determined upon comparison to the densities of separate KOH and separate KHS solutions:

$$\Delta d_{K_2S}([K^+]) = d_{K_2S}([K^+]) - 0.5(d_{KHS}([K^+]) + d_{KOH}([K^+])) \quad (27)$$

where $[K^+]$ (moles/liter solution), is the molar concentration of K^+ in an aqueous solution nominally containing only the salt indicated.

The concentration variation of Δd_{K_2S}, calculated according to equation (26), is presented in Figure 15. In Figure 15 for aqueous

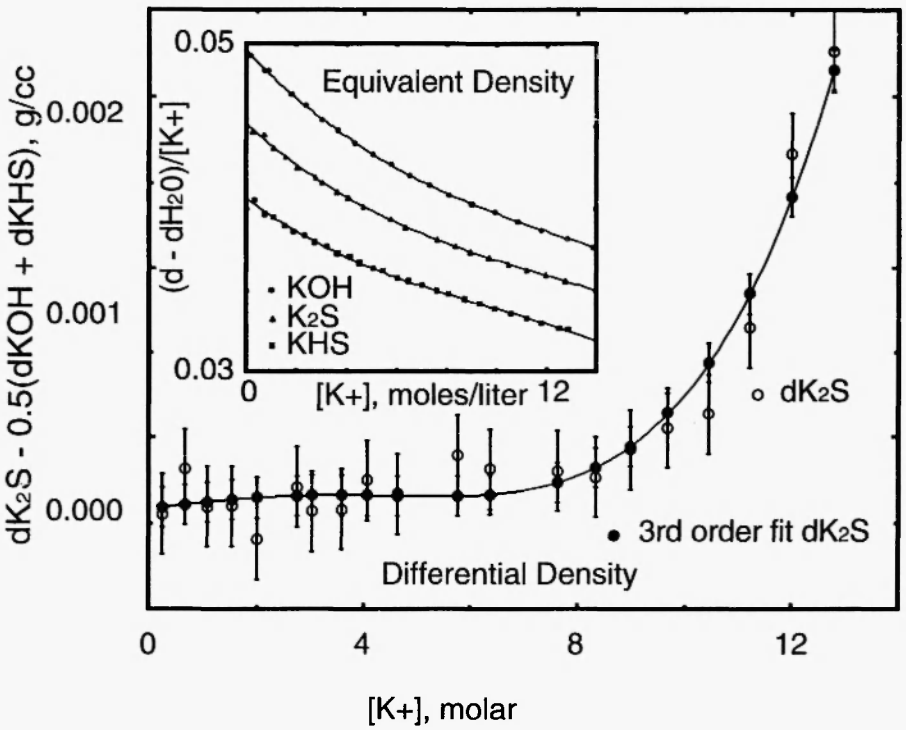

FIGURE 15 Differential density in aqueous concentrated alkaline potassium sulfide solutions at 25°C. The nominal molar concentration of each K_2S solution may be described as $C_{K_2S} = 0.5[K^+]$ or alternatively as a solution containing both $C_{KHS} = [K^+]$ and $C_{KOH} = [K^+]$. Δd_{K_2S} open circle points are calculated using direct experimental values of $d_{K_2S}([K^+])$, presented in Figure 1 inset. The Δd_{K_2S} solid circle points are calculated from a polynomial fit of experimental $d_{K_2S}([K^+])$ values. Inset: The equivalent density of concentrated KOH, K_2S or KHS aqueous electrolytes at 25°C, calculated from the measured density in accordance with equation (24).

electrolytes, nominally comprised of up to 3 **M** K_2S, it is evident that the solution density is comparable to solutions containing 50 percent isolated KOH and 50 percent isolated KHS, with no evidence of volume changes due to the reaction of HS^- and OH^- to form free sulfide. At concentrations increasing above 3 **M** K_2S, a significant increasing deviation of solution density, in excess of the solution density of the isolated reactants, is

evident. The observed increase in density is consistent with the formation of a more highly charged, and therefore more densely packed ion, such as S^{2-}.

The relative free sulfide in solution may be estimated by densometric comparison of K_2S solutions to pure equimolar solutions of KHS and KOH. Figure 16 presents the concentration variation of these predicted relative differential densities, assuming a range of hydrogen

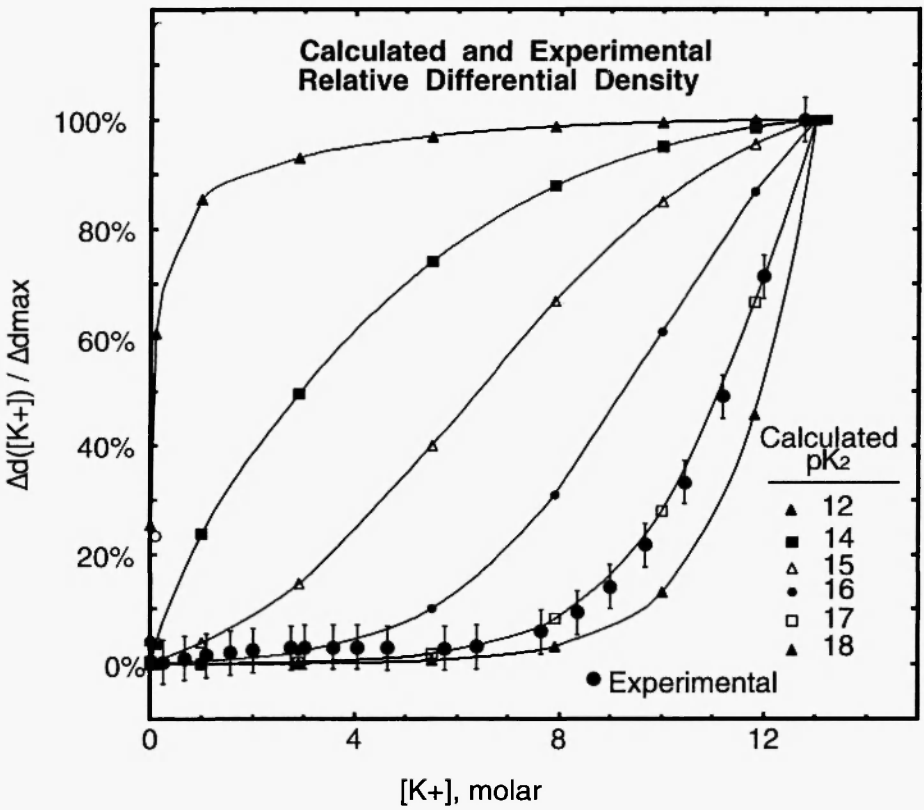

FIGURE 16 The calculated and experimental concentration dependence of the relative differential density of aqueous K_2S solutions at 25°C. Calculated and experimental values are compared to a maximum value of Δd_{K_2S} determined for 6.4 **M** K_2S. $[K^+]$ refers to the molar concentration of K^+ in an aqueous solution of K_2S. Calculated relative differential density is determined using $Kw = 1.00 \times 10^{-14}$, values of a_W and activity from Table 1, and assuming a hydrogen sulfide second acid dissociation constants varying from $pK_2 = 12$ to 18.

sulfide second acid dissociation constants varying from pK_2 = 12 to 18. These calculated values for $(\Delta d_{K_2S})_{relative}$ can be compared to experimental values for $(\Delta d_{K_2S})_{relative}$, determined using the measured values of $\Delta d_{K_2S}([K^+])$ and $\Delta d_{K_2S}([K^+]=12.8\ M)$ as summarized in Figure 15. In Figure 16 upon comparison of idealized and measured values of $(\Delta d_{K_2S})_{relative}$, it can be seen that a best fit of pK_2 = 17.1 ±0.3 provides an excellent simulation of the measured relative differential density for the complete range of K_2S concentrations studied.

D. Differential Densometric Benefits and Disadvantages

Densometric analysis, unlike potentiometric and spectroscopic analytic techniques, can not provide an absolute identification of the species being monitored. However, as opposed to other analytic techniques, which can exhibit increasing uncertainty with concentration, the physical analysis of solution density is particularly suited to concentrated solutions. The accuracy of density measurements is essentially concentration independent. Therefore in Figure 16, the effective signal to noise ratio of densometric analysis increases with increasing concentration. Combined with other techniques which qualitatively identify the relevant species in a concentrated liquid phase equilibrium, differential densometric analysis can provide a precise analysis of the equilibrated distribution of species. The example used illustrates application to unusually concentrated media, and demonstrates the advantage of this technique to probe liquid phase equilibria in this regime.

VI. SUB-MICRON PATH UV/VIS/IR SPECTROSCOPY

A. Conventional Absorption Spectroscopy Limits

The molar absorptivity of chromophores generally limit analysis, by absorption spectroscopy to concentrations of less than 1 molar. Higher concentrations result in absorption, A, greater than 2, and beyond the limit of conventional spectrophotometers. Direct path absorption studies are contingent on the simple Lambert-Bouguer linear relationship between light absorption and the path traversed, l. This combines in Beer's 1852 relationship between absorption, and concentration, C, to yield for a species of molar absorptivity, ε:

$$A = \log (I_0 / I) \propto \varepsilon \, l ; \qquad A = \varepsilon \, l \, C \qquad (28)$$

Spectroscopic absorption phenomena have been investigated over a tremendous range of spatial dimensions varying from astronomic distances down to molecular dimensions. In the smallest spatial domains the spectroscopy of adsorbed monolayers and Langmuir-Blodgett films of thickness on the order of angstroms has been widely probed. There has been a growing interest in the spectroscopy of thin films, by techniques using physical properties arising at surface interfaces, including diffraction [34], and reflectance and polarization enhancement [35,36].

In purely solution phase, there has been no analogous spectroscopic studies to the small dimensions used in thin film studies. Direct path ultraviolet, visible, or infrared absorption spectroscopy has been conducted with cells of pathlength down to several microns in the study of rapid kinetic measurements [37] and concentrated analytes [38], but due to material constraints there are few reports of liquid phase cells below one micron. Until recently, no systematic investigation of liquid phase absorption cells with dimensions smaller than the wavelength of incident radiation had been reported [3], although a sub-micron thickness thin film UV absorption spectra having a quite diffuse spectral structure (to a resolution of 900 cm^{-1}) has been reported [39]. This cell path length domain is intriguing for near ultraviolet, visible and infrared absorption spectroscopy. It is in this domain that the cell path length, and light pathway, approaches and actually becomes smaller than the dimensions of the wavelength of incident radiation.

Although literature references to sub micron pathlength liquid phase absorption spectroscopy are sparse, a variety of schemes have been investigated for producing sub wavelength illumination to deliver visible light to confined locations. These include channeling excitons to the point of illumination [40] or by propagation of photons through sub-micron apertures [41,42]. The significance of the micron domain in spectroscopy is evident in a Raman study in which spectroscopic cells of micron spatial resolution are presented to address molecular effects in single living cells [43]. Alternative, techniques to investigate in-situ liquid phase effects with a high degree of spatial resolution have been developed. These include X-ray diffraction to explore the structure of the electrochemical double layer [34], and microelectrode probes to map the movement of as few as 40,000 discrete ions [44].

B. Submicron Pathlength Cells

Cells of micron or submicron dimensions were fabricated by sandwiching appropriate plates (as described below) in a modified 0186-

0072 Perkin Elmer cell mount. Cells were assembled in a laminar flow chamber filled with prefiltered Ar. Solutions were prefiltered by injection through a syringe filter.

The 0.08 μm pathlength cell contained two EDMUND B43,400 precision single surface flats, fused quartz windows (1/20 wave (31 nm) flatness, 12.7 mm diameter, 3.18 mm thickness). 0.015 μm pore, 25 mm diameter membrane unit was used to filter both Ar and liquids. Two ESCO E210450 precision flat, fused quartz windows (1/10 wave (53 nm) flatness, 25.4 mm diameter, 6.35 mm thickness) were used for the 0.28 μm pathlength cell. in this case Ar was filtered by a 0.1 μm pore, 25.4 mm diameter membrane unit (Micron Separations DDN01025) and liquids were filtered by a 0.22 μm filter. Two ESCO Q10063 flat quartz plates, Two NaCl plates without a spacer and with a 25 μm Ag wire, Alpha 00307 spacer were used respectively for 0.56 μm 2.2 μm, 27.7 μm cells. 0.1 μm pore filter was used for Ar and 0.22 μm filter was used for liquids in the last three cases.

Perkin Elmer 1330 Infrared Spectrophotometer and Perkin Elmer Lambda 3B UV/Vis Spectrophotometer were used in spectral measurements. Chemicals were of analytical quality and used as received from commercial sources. Distilled deionized water was used in solution preparation.

C. Submicron Pathlength Absorption Spectroscopy

The spatial confinement of planar radiation is diffraction limited by the direction orthogonal to the direction of propagation [35]. Hence even in the domain in which the cell path length is smaller than the wavelength of incident radiation, the retention of spectral resolution is consistent with a large orthogonal cell width. In each absorption cell that was utilized, the orthogonal dimension (cell width) is more than 1000 thousand fold greater than the wavelength of incident radiation. Nevertheless, diffraction is expected at the sharp variation in index of refraction occurring at the interfaces from the (empty) dry cell. This effect is commonly used to calibrate IR cells. Alternately, in smaller dimension (micron and submicron) cells, if UV/vis radiation is employed, this diffraction can be used to quantify these small pathlength. The measurement of absorption within the dry cell results in a broad interference-fringe spectrum. Interference in a cell of pathlength, l, results in n fringes over a wavelength range from λ_1 to λ_2 [45]:

$$l = \frac{n\,\lambda_1\,\lambda_2}{2\,|\lambda_2 - \lambda_1|} \tag{29}$$

Two effects suggest that equation (28) interference within submicron cells by will not affect measured absorption spectrum in the solution phase. The amplitude of this interference diminishes to zero as the indices of refraction of window and solution components of the cell approach a single value. A maximum amplitude for an interference fringe spectrum occurs in the dry cell with a difference of indices of refraction = η(window) - 1. In each of the investigated liquid phase cells, η(window) - η(solution) < η(window) - 1. As expected no superimposed interference spectrum is observed in the cells containing solution samples. Secondly, in accordance with equation (29) the interference pattern broadens with decreasing cell width, and the number of interference cycles is no longer significant for pathlength < 100 nm in the UV/Vis/IR region.

Micron and submicron pathlength solution phase spectroscopy is sufficiently unusual to require independent measurements to confirm path length calibration. A second approach, in addition to that offered by interpretation of the observed interference in dry cells, may be derived from a consideration of the limiting parameters in very thin cells. Submicron pathlength thin cells can consist of sandwiched optically flat quartz disks in which particulate impurities have been reduced in the ambient environment, and can permit direct observation of solutions substantially more concentrated than with conventional cells. The cell pathlength is restricted by the specific flatness, f, of both of the two sandwiched optical windows and also the maximum size of particulate impurities present in the cell, p. The specific flatness is limited by either the roughness or the curvature of the optical window. Therefore, from the microscopic perspective, l represents only an average distance over plates separated by surface morphology, curvature and particulate impurities. The cell pathlength is limited by:

$$l = p + 2f \tag{30}$$

Finally, a third independent confirmation of path length calibration may be determined by comparison of the Lambert-Beer relationship, equation (27), for two cells i and j of different pathlengths. If cell j, has a calibrated pathlength, l_j, such as found in a conventional (longer pathlength) cell, than the unknown pathlength, l_i, is simply proportional to the concentration normalized absorption measured in each cell:

$$l_i = l_j C_j A_i / C_i A_j \tag{31}$$

Equations (28-30) can provide independent measurements of pathlength. Equation (29) recognizes that the pathlength arises from

the extremes in microscopic surface morphology of the optical plates and impurities which separate these plates. Equations (30) assumes a constant molar absorptivity over the concentration range studied.

D. Submicron Pathlength Examples

This section demonstrates near UV/Vis and IR absorption spectroscopy systematically reduced from the domain of conventional pathlength cells to the sub-micron domain. In this domain spectral resolution can be retained, and the applicability of equation (27) to pathlengths as short as 77 nm, is applied to the absorption of light of up to 3500 nm wavelength. Direct spectroscopic observation of concentrated high extinction coefficient species, and *in-situ* analysis of the equilibrium distribution of species in highly concentrated media are also demonstrated. Due to the unusually small pathlengths, cell volumes ($\sim 10^{-8}$ L) are small compared to the significant exposure area (~1 cm^2).

Figure 17 presents the visible absorption spectrum of a high extinction compound ($\varepsilon > 10^5\ M^{-1}\ cm^{-1}$), ß-carotene, in cells of conventional

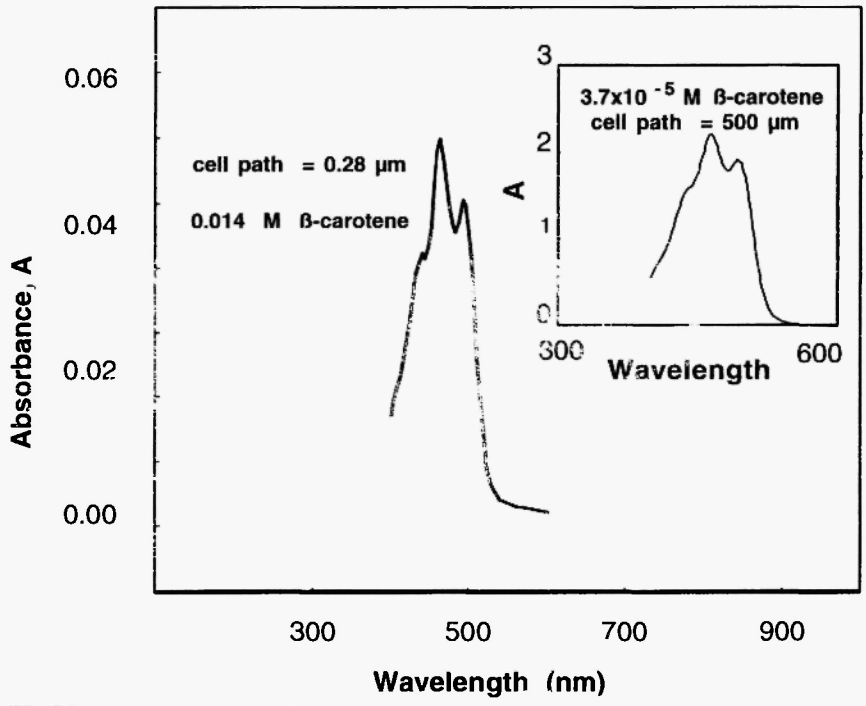

FIGURE 17 Absorption spectrum of benzene analytical grade solutions of ß-carotene in 0.28 µm and conventional 0.5 cm (inset) cells.

and sub-micron pathlengths. As seen in the inset of Figure 17, and as a result of the high molar absorptivity of ß-carotene, spectra may be observed in a 0.5 cm pathlength quartz cell for ß-carotene in solution of concentrations only below $5x10^{-5}$ **M**. Alternatively sub-micron pathlength cells will allow direct observation of substantially more concentrated solutions of ß-carotene. As seen in Figure 17, the spectrum of a saturated (0.014 **M**) ß-carotene in benzene is obtained in a cell in which the pathlength is reduced by four orders of magnitude to 0. 3 μm. The cell pathlength is determined from the inset of Figure 18 by interference-fringe, equation (28), as 0.28 μm, by particulate limitation, equation (29) (f = 0.05μm and p =0.22 μm), as 0.32 μm, and by the Lambert-Beer relation, equation (30), as 0.31 μm. Application of equation (30) to N-N dimethyl-p-toluidine (ε_{254nm} = 12,500 $M^{-1}cm^{-1}$) and benzaldehyde (ε_{243nm} = 14,000 $M^{-1}cm^{-1}$) solutions in the same macroscopic and

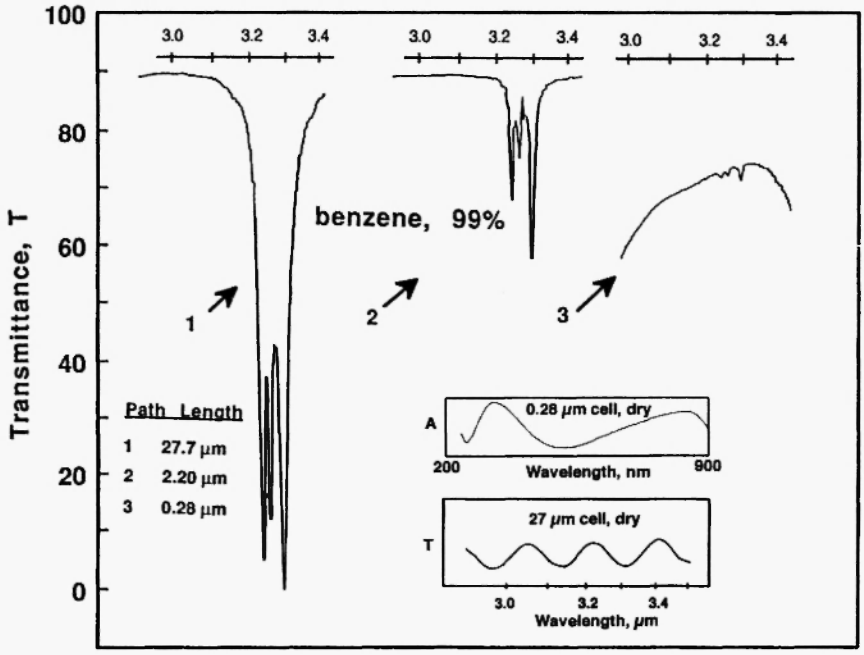

FIGURE 18 IR transmission spectrum of benzene in 27.7(±1) μm, 2.2(±0.3) μm and 0.28(±0.03) μm pathlength cells. Pathlengths were determined from Eq. 3 and the average of several interference patterns as exemplified in the insets for 27.7 μm cell and 0.28 μm sub-micron cells.

microscopic cells described in Figure 17, determine the pathlength to be 0.28 and 0.21 μm respectively.

The fused silica transmission window is highly transparent from 2.8 to 3.6 μm radiation. This transmission window may be used to study sub-micron pathlength IR spectroscopy, and retention of spectral resolution in this pathlength domain. Benzene has several closely spaced C-H stretch bands in this region, and Figure 18 presents the infrared transmission spectrum of benzene in conventional and sub-micron pathlength cells. In each cell, including the 0.28 μm pathlength cell, it is seen that the C-H absorption peaks are resolved to within 6 cm^{-1} approaching the instrumental resolution. Shifts in peak position have been calculated to be significant for cell window materials of various indices of refraction, but are generally small (< 5 cm^{-1}) [46].

Benzene absorptivity of 3 μm light is of insufficient magnitude to discern absorption spectra in cells of pathlength less than 0.2 μm. Absorption spectra are investigated in cells systematically reduced to even shorter pathlengths using cyclohexane with an order of magnitude higher absorptivity in the available transmission window ($\varepsilon_{3.41\mu m}$ = 300 $M^{-1}cm^{-1}$), and are presented in Figure 19. In accordance with equation (28), the 0.08 (0.077) μm pathlength cells evidence no discernible interference spectrum, and the optical pathlength was determined from equation (29) for these cells (using p = 15 nm and f= 31 nm). Figures 17 - 19 present data demonstrating the continuity of spectral shape, resolution and position for cell pathlengths substantially less than the wavelength of radiation incident upon the cell.

Figure 19 illustrates the validity of Lambert-Bouguer relations in sub micron pathlength domain. The 0.077 μm pathlength cell has a pathlength a factor of 44 shorter than 3.41μm wavelength of incident radiation used to measure the cyclohexane spectrum in Figure 19. No evidence of chemisorption was observed in these cells. The inset of Figure 19 presents the variation of the measured absorption from 28 μm down to 0.08 μm cell pathlengths. The data presented in the Figure 19 inset extends the Lambert-Bouguer linearity of absorption amplitude with cell pathlength, equation (27), down to the cell pathlength domain of less than 10^{-7} m.

The demonstrated linearity of absorption with pathlength variation and no evidence of chemisorption excludes the possibility that adsorption, chromophore orientation, or applied electric fields have been used to enhance effective light absorption. Therefore it can be noted, that the results summarized in Figures 20 and 21 relate solely to bulk chromophore, and not perturbed or oriented chromophore, properties.

Shorter path length cells also permit absorption spectroscopy of increasingly concentrated aqueous solutions. For example as shown in

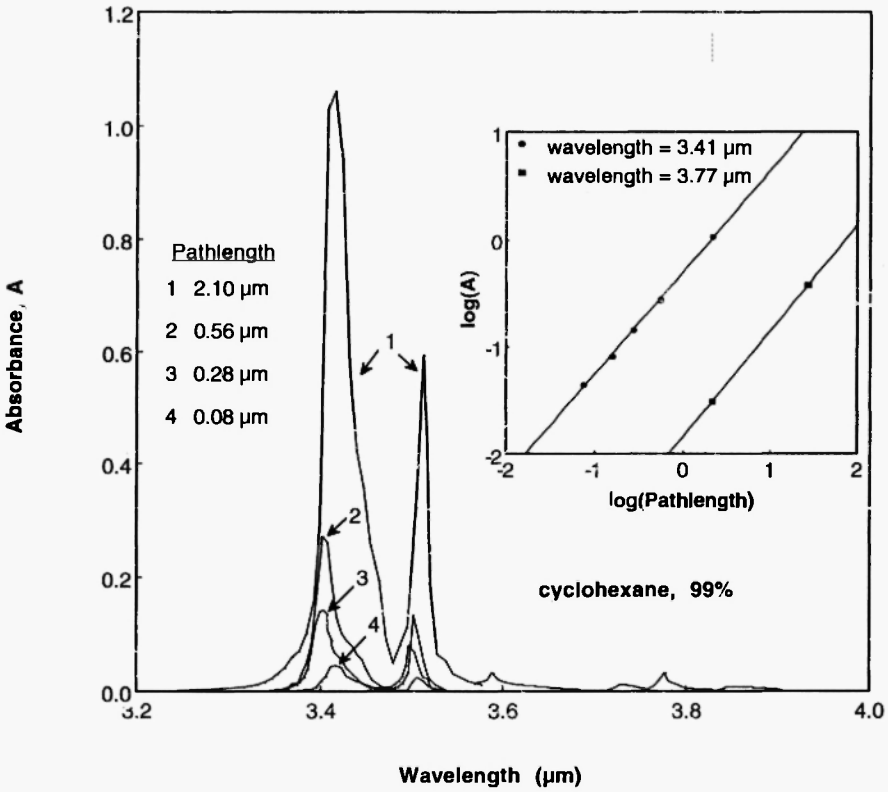

FIGURE 19 IR absorption spectra of cyclohexane in 2.2(±0.3), 0.56(±0.06), 0.28(±0.03) or 0.08(±0.01) μm pathlength cells. Inset: Variation of the indicated cyclohexane absorption maxima from pathlengths of 27.7 μm down to 0.077 μm. Inset contains 0.162 μm path length cell data, configured as in the 0.077 μm cell, but utilizing a larger 0.10 μm pore, 25 mm diameter membrane unit. 27.7 μm pathlength data exceeds the absorption range at shorter wavelengths, and is not included in the main figure.

Figure 20, a 13 μm pathlength cell, permits detection of the near UV spectrum of 0.3 **M** K_2S, with or without 13 **M** added KOH. While, as shown in Figure 21, an 0.28 μm pathlength cell, permits near UV absorption spectroscopy of over 6 **M** K_2S or KHS solutions [3].

VII. FINAL COMMENTS

This paper has discussed the theory and experimental methodology of several techniques applicable to the analysis of

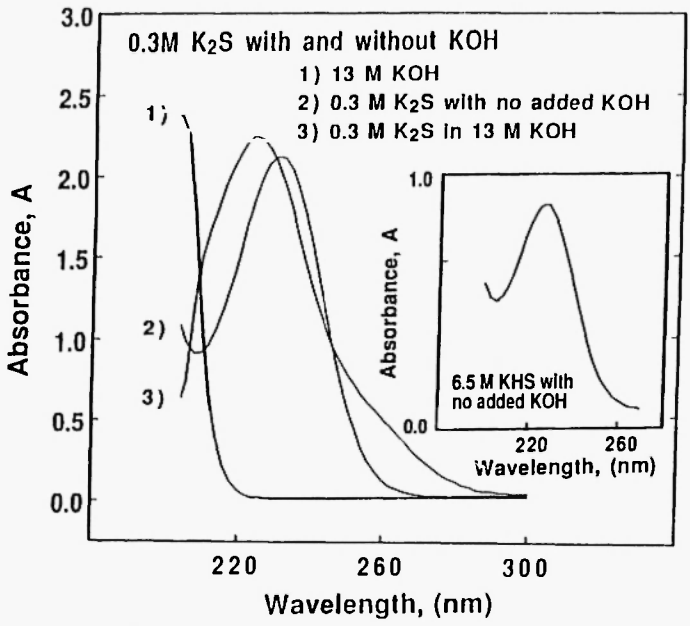

FIGURE 20 Near UV spectroscopy of concentrated KOH and KHS solutions in a 13 μm pathlength cell. Inset: Concentration variation of peak absorption in KHS (figure inset) or equimolar KHS/KOH solutions.

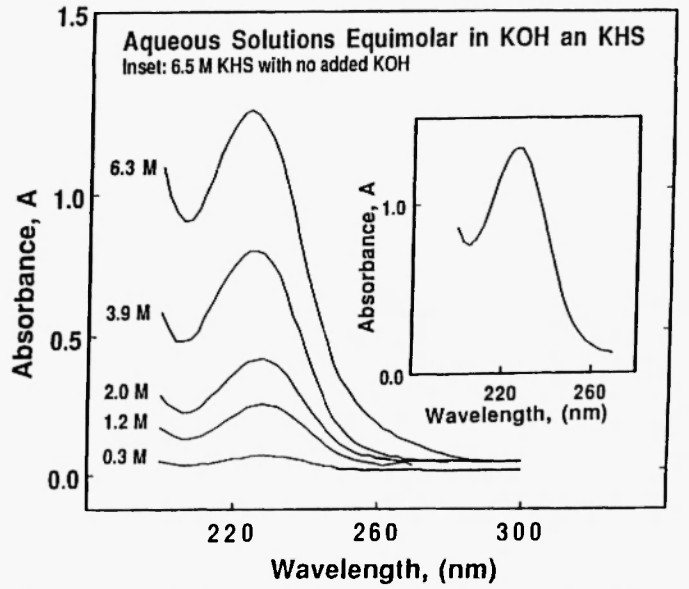

FIGURE 21 Near UV spectroscopy of solutions containing equimolar aqueous KHS and KOH in a 0.28 μm pathlength cell.

concentrated electrolytes. The analysis of concentrated electrolytes poses fundamental and practical challenges. Yet, successful methodologies to analyze these solutions are of importance to understand chemical processes occurring in the concentrated solution phase, and are applicable to on-line analysis of industrial processes, as well as environmental analysis of concentrated toxic effluents. Successful new analytical techniques for analysis of these solutions will be based on physical chemical properties which tend to be accentuated, rather than obscured, with increasing salt concentrations.

VIII. ACKNOWLEDGMENTS

Several of the analytical methodologies presented in this paper were developed together with research students and fellows in my laboratory including F. Forouzan, D. Peramunage and K. Longo. The author is grateful for partial support for this project by the Israel Academy, and by the Technion V.P.R. Fund and the Fund for the Promotion of Research at the Technion.

IX. REFERENCES

1. S. Licht, F. Forouzan, and K. Longo, *Anal. Chem., 62*: 1356 (1990).
2. S. Licht, D. Peramunage, F. Forouzan, and K. Longo, "Novel Analytical Techniques for Super Concentrated Electrolytes" in Proc. of the Symposia on Electrochemical Engineering, C. W. Walton Editor, *Electrochem. Soc. Proc. Vol. 90-10*: 241 (1990).
3. D. Peramunage, F. Forouzan, and S. Licht, *Anal. Chem., 66*: 378 (1994).
4. R. G. Bates, *Determination of pH*, Wiley, New York, 1964.
5. M. W. Lovell, *Anal. Chem., 55*: 963 (1983).
6. J. R. Jones, *Chem. Brit., 7*, 336 (1971).
7. *Glass Electrodes for pH and Other Cations*, G. Eisenman, Ed.; Marcel Decker, New York, 1967.
8. S. Licht, *Anal. Chem., 57*: 415 (1985).
9. J. F. Wojclk, *J. Phys. Chem., 71*: 145 (1982).
10. G. Ackerlof and P. Bender, *J. Amer. Chem., 70*: 2366 (1948).
11. W. J. Hammer, *Trans. Electrochem Soc., 72*: 45 (1937).
12. R. G. Picknett, *Trans. Faraday Soc., 64*: 1059 (1968).

13. G. Mattlock, *Advances in Analytical Chemistry and Instrumentation, Vol. 2*, Wiley, New York, 1963.
14. L. Kratz, *Glastech. Ber., 28*: 35 (1950).
15. G. Mattlock, *pH Measurement and Titration*, Heywood: London, 1961.
16. D. Hubbard, G. F. Rynders, *Natl. Bur Stand, 39*: 561 (1947).
17. S. Licht, and J. Manassen, *J. Electrochem. Soc., 134*: 918 (1987).
18. S. Licht, Aqueous Solubilities, *J. Electrochem. Soc., 135*: 2971 (1988).
19. A. N. Kirgintsev, A. V. Luk'yanov, *Zhurnal Neorganicheskovi Khimii, 12*, 2032 (1967).
20. Lange's Handbook of Chemistry, 13th ed., J. A. Dean, Editor, McGraw-Hill, Inc., New York, 1985.
21. (a) R. H. Stokes Chapter 1 in *Activity Coefficients in Electrolyte Solutions*, Vol. 1; R. M. Pytkowicz, Ed; CRC Press: Boca Raton, FL, 1981; (b) Platford, R. F., Chapter 3, *ibid*; (c) Butler, J. N., Chapter 4, *ibid*; (d) Desnoyers, J. E., Chapter 6, *ibid*. (e) *ibid*, Vol.2.
22. W. R. Bousfield, *Trans. Faraday Soc.* (1917).
23. D. A. Sinclair, *J. Phys. Chem., 37*, 495 (1933).
24. R. H. Stokes, *J. Amer. Chem. Soc., 69*, 1291 (1947).
25. A. T. Williamson, *Proc. R. Soc. Edinburgh Sect. A., 195*, 97 (1948).
26. R. A. Robinson, *J. Phys. Chem., 73*, 3165 (1969).
27. H. Braunstein and J. Braunstein, *J. Chem. Thermodyn., 3*, 419 (1971).
28. F. Forouzan and S. Licht, *Anal. Chem., 66*: 2003 (1992).
29. T. S. Light, Electrodeless Conductivity , in *Electrochemistry, Past and Present, ACS Symp. Series 390*, 429 (1989).
30. T. S. Light, E. S. Atwood, J. Driscoll and S. Licht, *Anal. Chem., 65*, 181 (1993).
31. T. S. Light, S.Licht, *Anal. Chem., 59*, 2327 (1987).
32. D. Peramunage and S.Licht, *Solar Energy*, 52, 197 (1994).
33. S. Licht, K. Longo, D. Peramunage and F. Forouzan, *J. Electroanal. Interf. Electrochem., 318*: 111 (1991).
34. M. J. Bedzyk, G. M. Bommarito, M. Caffrey, T. L. Penner, *Science 248*, 52 (1990).
35. F. Oznam, J-N. Chazalviel, *Rev. Sci. Instrum. 59*, 242 (1988).
36. R. S. Mcdonald, *Anal. Chem. 58*, 1906 (1986).
37. C. S. Yoo, Y. M. Gupta, *J. Phys. Chem. 94*, 2857 (1990).
38. W. Giggenbach, *Inorg. Chem. 10*, 1333 (1971).
39. T. Inagaki, *J. Chem. Phys. 57*, 2526 (1972).
40. K. Lieberman, S. Harush, A. Lewis, R. Kopelman, *Science 247*, 59 (1990).
41. E. Betzig, A. Lewis, A. Harootunian, M. Isaacson, E. Kratschmer, *Biophys. J. 49*, 269 (1986).

42. A. Harootunian, E. Betzig, M. Isaacson, A. Lewis, *App. Phys. Lett. 49*, 674 (1986).
43. F. G. Puppels, F. F. M. de Mul, C. Otto, J. Greve, M. Robert-Nicoud, D. J. Arndt-Jovin and T. M. Jovin, *Nature 347*, 301 (1990).
44. S. Licht, V. Cammarata, M. S. Wrighton, *Science 243*, 1176 (1989).
45. D. C. Smith and E. C. Miller, *J. Opt. Soc. Amer. 34*, 130 (1944).
46. H. J. K. Koeser, *Fresenius' Z. Anal. Chem. 317*, 845 (1984).